

**VIETNAM GENERAL CONFEDERATION OF LABOUR
TON DUC THANG UNIVERSITY
FACULTY OF ELECTRICAL AND ELECTRONIC ENGINEERING**



PHONG THANH TRAN

**LOAD FREQUENCY CONTROL IN
MULTI-AREA INTERCONNECTED
POWER SYSTEM USING SLIDING
MODE CONTROL**

**DOCTORAL DISSERTATION OF
ELECTRICAL ENGINEERING
(SUMMARY)**

HO CHI MINH CITY, JANUARY YEAR 2024

**VIETNAM GENERAL CONFEDERATION OF LABOUR
TON DUC THANG UNIVERSITY
FACULTY OF ELECTRICAL AND ELECTRONIC ENGINEERING**



PHONG THANH TRAN

**LOAD FREQUENCY CONTROL IN
MULTI-AREA INTERCONNECTED
POWER SYSTEM USING SLIDING
MODE CONTROL**

**DOCTORAL DISSERTATION OF
ELECTRICAL ENGINEERING
(SUMMARY)**

Advised by

Dr. Huynh Van Van

Dr. Dong Sy Thien Chau

HO CHI MINH CITY, JANUARY YEAR 2024

ABSTRACT

Achieving and maintaining stable operation in power systems (PS) is a challenging task that aims to satisfy both consumers and suppliers. Control and stability in power systems involve addressing various challenges. To ensure stable operation, different control loops are implemented to regulate different parameters. For instance, Load Frequency Control (LFC) or Automatic Generation Control (AGC) is utilized to keep the frequency close to its nominal values. In addition, that control loop has the charge of upholding the scheduled power exchange between interconnected control areas through tie-lines. The focus of this thesis is on addressing in multi-area power system (MAPS):

First, the utilization of SMC in LFC of power network (PN) poses challenges because of the chattering phenomena connected to high-frequency switching. These chattering issues can be highly detrimental to actuators employed in PS. The suggested approach, known as second order integral sliding mode control (SOISMC), not only effectively eliminates chattering in the control input but also ensures the multi-area PN's adaptability. A novel LMI technique is derived to guarantee the stability of whole system via Lyapunov theory. Additionally, the results obtained from simulations highlight the suitability of the proposed SOISMC for practical implementation in multi-area PN, where it effectively mitigates high parameter uncertainties and load disturbances, time-delay communication.

Second, in response to the escalating demand for electricity and the need to balance the total generated power, addressing this, the LFC of the two-area gas-hydro-thermal power system (TAGHTPS) is presented through the application of a single-phase sliding mode control-based state observer (SPSMCBSO). This approach offers several notable contributions. Firstly, the TAGHTPS model accounts for uncertainties in both parameter and interconnected matrix states. Secondly, a state observer is utilized to determine the state variables, enhancing feedback control. Thirdly, the SPSMCBSO technique modifies the conventional SMC, thereby improving TAGHTPS performance in the context of overshoot and time for settling. A stability evaluation of TAGHTPS is conducted using a novel linear matrix inequality (LMI) scheme based on the hypothesis of stability proposed by Lyapunov. Finally, the experiment's outcomes are presented and compared against reputable traditional control techniques, the SPSMCBSO further demonstrated robustness and is not affected by subsystem parameter deviation, random load disturbance, and parameter uncertainty in state and interconnected matrix, the inherent fluctuations in renewable energy sources.

Last, this research introduces a novel LFC approach employing a second order

sliding mode control with double integrated sliding surfaces (SOSDISS) , aiming to enhance frequency regulation, tie-line power management, and overall system reliability of the MAPS. Notably, this method not only enhances the asymptotic stability and dependability of the MASHPS but also mitigates the inherent presence of the chattering phenomenon in first order SMC. Additionally, the study employs a new LMI based on Lyapunov stability to comprehensively analyze the stabilization of the entire power system. To assess the efficiency of the suggestion's strategy for LFC, a two-area steam-hydropower system (TASHPS) is investigated. Through simulations, the effectiveness and reliability of the suggested control scheme are demonstrated through its rapid frequency responses and its resilience to factors such as parameter fluctuations, load disturbances, load variations, delay time, and the nonlinearity effects of governor dead band (GDB) and generation rate constraint (GRC), IEEE 39 bus on the PN.

KEYWORDS: Power system, Sliding mode control, Load frequency control, Automatic generation control, Time delay communication, Governor dead band (GRC), Generation rate constraint (GRB), Wind plant, Time delay communication.

LIST OF PUBLISHED PAPERS BY AUTHOR

1. Huynh, Van Van, **Phong Thanh Tran***, Bui Le Ngoc Minh, Anh Tuan Tran, Dao Huy Tuan, Tam Minh Nguyen, and Phan-Tu Vu. "New second-order sliding mode control design for load frequency control of a power system." *Energies* 13, no. 24 (2020): 6509 (**ISI**).
2. Huynh, Van Van, **Phong Thanh Tran***, Tien Minh Nguyen, Van-Duc Phan, and Viet-Thanh Pham. "Advanced sliding mode observer design for load frequency control of multiarea multisource power systems" *International Transactions on Electrical Energy Systems* (2022) (**ISI**).
3. Van Van Huynh, **Phong Thanh Tran***, and Chau Si Thien Dong, Bach Dinh Hoang, "Sliding surface design for sliding mode load frequency control of multi area multi source power system", *IEEE Transactions on Industrial Informatics*, 2024 (**ISI**).
4. **Phong Thanh Tran**, Van Van Huynh and Chau Si Thien Dong, Bach Dinh Hoang, "Automatic generation control based sliding mode observer design for multi-area multi-source power systems", the 7th International Conference on Advanced Engineering – Theory and Applications, 2022.
5. **Phong Thanh Tran**, Van Van Huynh, Chau Thien Si Dong, and Bach Hoang Dinh. "Sliding mode-based load frequency control of a power system with multi-source power generation" In 2023 International Conference on System Science and Engineering (ICSSE), pp. 142-147. IEEE, 2023.
6. Tran, Anh-Tuan, Bui Le Ngoc Minh, **Phong Thanh Tran**, Van Van Huynh, Van-Duc Phan, Viet-Thanh Pham, and Tam Minh Nguyen. "Adaptive integral second order sliding mode control design for load frequency control of large-scale power system with communication delays" *Complexity* 2021 (2021) (**ISI**).
7. Van Huynh, Van, **Phong Thanh Tran**, Tuan Anh Tran, Dao Huy Tuan, and Van-Duc Phan. "Extended state observer-based load frequency controller for three area interconnected power system" *TELKOMNIKA (Telecommunication Computing Electronics and Control)* 19, no. 3 (2021): 1001-1009 (**Scopus**).
8. Huynh, Van Van, Bui Le Ngoc Minh, Emmanuel Nduka Amaefule, Anh-Tuan Tran, and **Phong Thanh Tran**. "Highly robust observer sliding mode-based frequency control for multi area power systems with renewable power plants" *Electronics* 10, no. 3 (2021): 274 (**ISI**).
9. Tran, Anh-Tuan, Bui Le Ngoc Minh, Van Van Huynh, **Phong Thanh Tran**, Emmanuel Nduka Amaefule, Van-Duc Phan, and Tam Minh Nguyen. "Load frequency regulator in interconnected power system using second order sliding mode control combined with state estimator" *Energies* 14, no. 4 (2021): 863 (**ISI**).
10. Huynh, Van Van, Bui Le Ngoc Minh, Emmanuel Nduka Amaefule, Anh-Tuan Tran, **Phong Thanh Tran**, Van-Duc Phan, Viet-Thanh Pham, and Tam Minh Nguyen. "Load frequency control for multi-area power plants with integrated wind resources" *Applied Sciences* 11, no. 7 (2021): 3051 (**ISI**).

11. Tran, Anh-Tuan, **Phong Thanh Tran**, and Van Van Huynh. "Load frequency control for power system using generalized extended state observer" *Journal of Advanced Engineering and Computation* 5, no. 1 (2021): 1-18.

CHAPTER 1. INTRODUCTION

1.1. The motivation

The electrical PS, the conventional electrical system was structured around this framework. Utility companies were responsible for the entire process of electricity generation, transmission, and distribution within their designated areas, known as balancing or control areas. Consequently, the design and control requirements for this system were well-established and reasonably manageable in terms of complexity. The ongoing transformation within the PS is closely tied to advancements in information and communication technology. This progression is anticipated to shape a future power system characterized by several key attributes. These include the capacity to integrate emerging generation technologies, optimize the utilization of network assets, adapt to evolving market dynamics, prioritize environmental sustainability, and enhance overall grid efficiency, safety, and reliability. This shift in the power landscape, accompanied by the growing intricacies of the grid, is illustrated in Figure 1.1 (Willis, H. L., & Philipson, L., 2018).

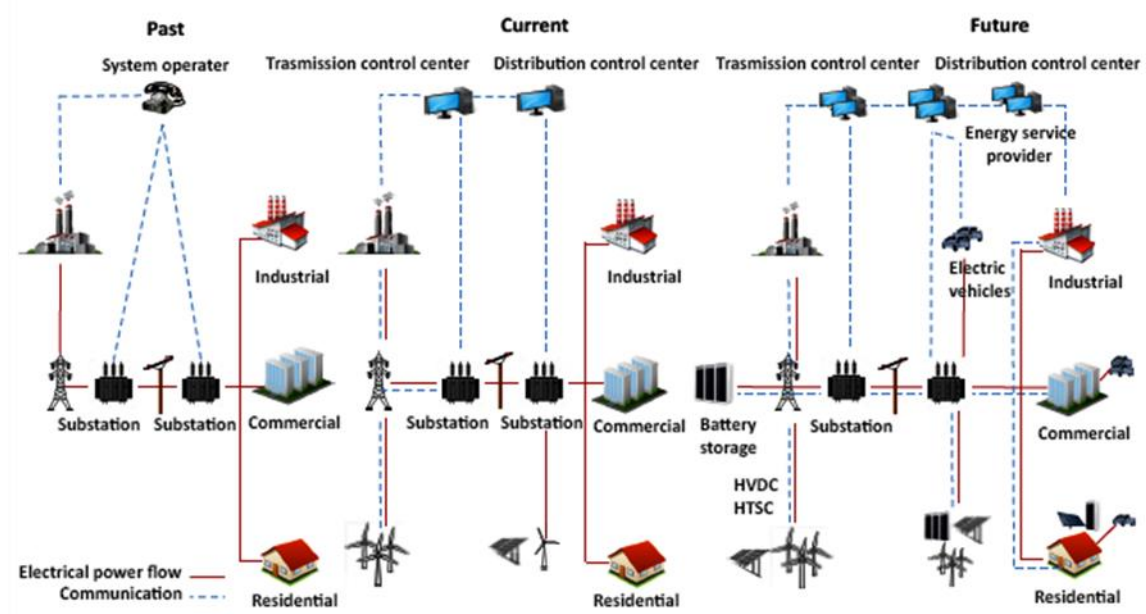


Figure 1.1. The evolutionary process of the transition to a future smart grid

To ensure the effective operation of the future grid, specific enabling technologies are essential (Edris, A. A., & D'Andrade, B. W., 2017). The primary objectives of the LFC loop in PS are twofold. Firstly, it ensures the provision of required power from generation plants to meet fluctuating load demands. Secondly, it maintains the interchanged power at predetermined values among interconnected control areas (CA). By achieving these objectives, the LFC loop contributes to enhancing PS stability. It aims to eliminate steady-state errors in tie-line power

deviation and frequency fluctuation.

1.2. The objectives of the research

In this research, maintaining a constant frequency is essential for ensuring the efficient operation of a PS. Variations in frequency can have detrimental effects on PS performance, reliability, and efficiency. Substantial fluctuations in frequency can lead to equipment damage, degradation of load performance, overloading of transmission lines, and disruptions in system protection mechanisms. Frequency variations also have an adverse impact on the speed control and the operation of both induction and synchronous machines.

Should an abrupt load change transpire within a control region of an interconnected power system, it will result in fluctuations in frequency and tie-line power. The objectives of this research are following:

1. To preserve the actual frequency and the specified control yield (megawatt) in the connected power frameworks.
2. To regulate the change in tie-line power between regulated regions.

1.3. Scope of the research

In the scope of this research, LFC is concentrated and investigated. In a stable, dependable, and secure PS, it's crucial to swiftly restore the frequency and tie-line power flow between interconnected regions to their predetermined values after a load disturbance and uncertainty. This is accomplished by synchronizing the generated power with the demand while considering losses. This control method, referred to as LFC, enables synchronous generators to adapt their output to meet load requirements, ensuring that fluctuations and discrepancies in area frequency and tie-line power converge to zero. The MATLAB/SIMULINK software serves as a valuable tool for optimizing the performance of controllers, particularly in simulation scenarios. This involves employing straightforward and effective optimization techniques to identify the optimal values for the recommended parameters of the controllers. Through simulation, these techniques help fine-tune controller settings, ensuring that the system operates at its best possible performance.

1.4. Research methodology

In a more comprehensive examination, to assess the effectiveness and suitability of the proposed LFC systems, these methods are applied to various multi-area PS with multiple sources under diverse operating conditions. To attain the objective, the detailed following procedures are undertaken:

1. To perform an extensive examination of LFC, delve into the significant discoveries, current research areas, and potential problems, along with their corresponding solutions, pertaining to frequency fluctuations within contemporary PS.
2. To design and implement a new second-order integral sliding mode control (SOISM) inside the streamlined multi-area PS, with filtered derivative reactions for LFC and dual area interconnected PS, where it effectively mitigates high parameter

uncertainties and load disturbances, time-delay communication.

3. To create new integral surface SMC control designs, specifically a single-phase sliding mode control-based state observer (SPSMCBSO), to effectively regulate frequency in the experiment involving a two-area multi-source PS, such as the gas-hydro-thermal power system, while ensuring power interchanges remain within predefined boundaries.

4. To introduce the suggestion of a new design for second order SMC with double integral sliding surface (SOSDISS) and provide a comprehensive mathematical derivation. This design is intended for use in multi-source system models, specifically those representing the two-area gas-hydro-thermal power system (TAGHTPS).

5. The stability of various power systems is investigated utilizing novel LMI techniques grounded in Lyapunov stability theory.

6. To figure out how to optimize the performance of the controllers such as the SOISM, SPSMCBSO, SOSDISS in simulation by using MATLAB/SIMULINK, the straightforward and effective optimization techniques, are utilized to determine the optimal values for the recommended controllers' parameters.

7. To conduct an in-depth evaluation of the resilience and effectiveness of the suggested control approaches, a thorough examination is performed. This involves subjecting the system to various operating conditions and subsequently comparing the outcomes with control techniques that have been previously recommended.

1.5. New contributions of the research

The objective of this thesis is to explore the possibility of creating robust LFC systems with the goal of enhancing the dynamic performance of multi-area PS. This involves ensuring that the frequency variation and tie-line power deviations remain within acceptable limits, even in the event of disturbances.

The significant contributions of this research are as follows:

- To formulate and implement the novel control strategies referred to as second-order integral sliding mode control (SOISM) in the studied multi-area power models for LFC.

- To accomplish an innovative design and utilization of a single-phase sliding mode control-based state observer (SPSMCBSO) for the purpose of LFC in the context of a two-area gas-hydro-thermal power system (TAGHTPS).

- To employ the novel technique of a second order SMC with double integrated sliding surfaces, aiming to enhance frequency regulation, tie-line power management, and overall system reliability of the MASHPS. To put into practice a novel LFC approach tailored for a multi-area steam-hydropower system (MASHPS) under parameter uncertainty and various conditions.

1.6. Organization of the study

This part provides an overview of the arrangement and the primary focus of each chapter within this dissertation.

Chapter 1: This part furnishes the background of the subject, research methodology, research goals, objectives, contributions, and the study's purpose, along

with the problem statement.

Chapter 2: In this chapter, an extensive and current literature review is presented, covering various dimensions of LFC in PS, including considerations like system size, types, proposed LFC methods, and strategies. Each section within this chapter is assessed, and a concise summary is provided.

Chapter 3: Design of a new second order sliding mode control for power system load frequency control.

Chapter 4: Designing an advanced sliding mode observer for load frequency control in multi-area multi-source power systems.

Chapter 5: Sliding surface design for sliding mode load frequency control of multi area multi source power system.

Chapter 6: This chapter offers a summary of the thesis, outlines its conclusion, and lays out a clear direction for future research endeavors.

CHAPTER 2: LITERATURE REVIEW

This part presents a comprehensive and current review of LFC in both traditional and modern PS. It begins with an overview of LFC and proceeds to explore the characteristics of different PS configurations. The chapter also examines various control strategies employed for LFC, including centralized and decentralized approaches. Furthermore, it discusses LFC schemes based on traditional, optimal, adaptive, robust, and soft computing methods using artificial intelligence.

2.1. Power system

In extensive PS, which consists of multiple interconnected control regions, the primary goal is to ensure the consistent generation and distribution of power while maintaining critical parameters like frequency and voltage within acceptable ranges. The most common approach to address frequency variations is hierarchical control, typically classified into three tiers: primary control, secondary control, and tertiary control levels (Bevrani, 2014). In cases where the frequency deviates significantly from its nominal value, there might also be a requirement for an emergency control loop to reestablish the PS's frequency (F. M. Gonzalez-Longatt and J. Luis Rueda, Eds., 2014). Under typical operating conditions, minor fluctuations in frequency are mitigated by primary control, which acts over a period of several seconds. In situations where there are more substantial deviations in frequency (during abnormal operation) and depending on the available reserve power, a SCL, also referred to as LFC, is implemented to bring back the regularity of frequency. This process may take several minutes. Nevertheless, during situations characterized by significant imbalances between the power generation and the load demand resulting from a major fault, the restoration of frequency to its nominal value using the LFC loop may not be feasible. During such occurrences, tertiary control mechanisms become essential.

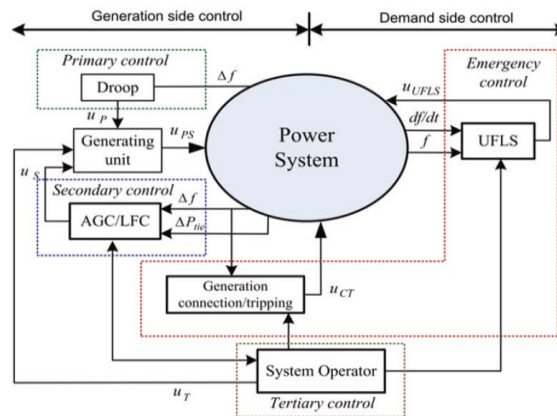


Figure 2.1. Control loops for frequency regulation within a PS

Beyond that, response to emergencies services is used to alleviate or reduce the risk of cascading failures (see Figure 2.1) (Bevrani, 2014). Building upon the preceding information, LFC or AGC emerges as a vital service crucial for ensuring the effective operation of PS (H. Bevrani and T. Hiyama, 2017).

2.2. Modelling of frequency response and dynamic model

The PS's frequency is contingent on the balance of real power. Any alteration in real power demand within the network affects the entire system by causing a shift in frequency. Consequently, system frequency serves as a valuable indicator of the balance of system power production and load. The control of real power output from a generator is contingent upon the mechanical power generated by the prime mover, which can be a steam turbine, gas turbine, hydro turbine, or diesel engine, depending on the type of generation. In instances involving steam or hydro turbines, the adjustment of mechanical power is achieved by manipulating valves that regulate the intake of steam or water flow into the turbine. It is imperative to continually manage the supply of steam (or water) to the generators to align it with the real power demand; otherwise, variations in machine speed will ensue, resulting in a shift in frequency. To guarantee the effective operation of a PS, it is crucial to maintain a nearly constant frequency (P. M. Anderson and A. A. Fouad, 2008). Besides primary frequency control, many large synchronous generators are outfitted with a secondary frequency control loop. In Figure 2.2, the speed governor identifies alterations in speed (frequency) through both the primary and secondary control loop.

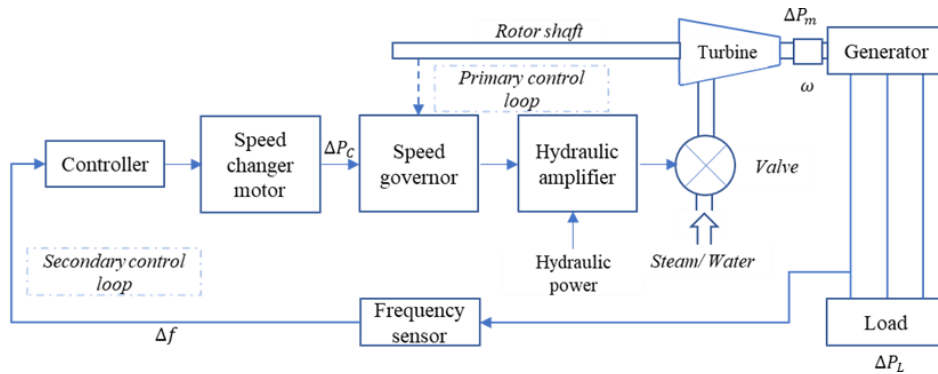


Figure 2.2. Block diagram representation of a synchronous generator with fundamental frequency control loops

In this research, we focus on the secondary control loop or load frequency control applying for variety of multi-area power system.

2.2.1 Secondary control loop or load frequency control

Large synchronous generators often incorporate an SFC loop in addition to the PFC. The schematic block diagram for the generator illustrates both the main and SFC loops (Bevrani, 2014). The additional loop introduces feedback to the PFC through a dynamic control scheme, utilizing the frequency offset as the feedback signal. This received signal is employed to adjust the system's frequency. In practical PS, the dynamic control scheme is typically a basic integral or proportional integral control scheme. After a load change, this feedback provides the turbine with the appropriate signal ΔP_m for load monitoring and restoring the SF, as depicted in Figure 2.3. (Bevrani, 2014).

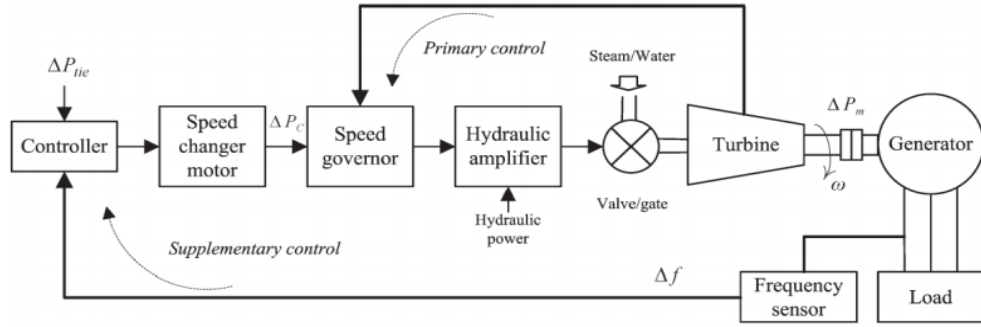


Figure 2.3. Governor-turbine with secondary frequency control loop

2.2.2 Frequency control in an interconnected power system

There's also the possibility of grouping multiple control areas into a larger single CA, where these larger areas operate in coordination with one another. These individual control areas are interconnected by tie lines, allowing for the exchange of power between them, often based on predetermined agreements that consider the operating costs of the selling utility (Alhelou, H. H., Hamedani-Golshan, M. E., Zamani, R., Heydarian-Forushani, E., & Siano, P., 2018). To illustrate this, refer to Figure 2.4, which illustrates a PS comprising N control areas:

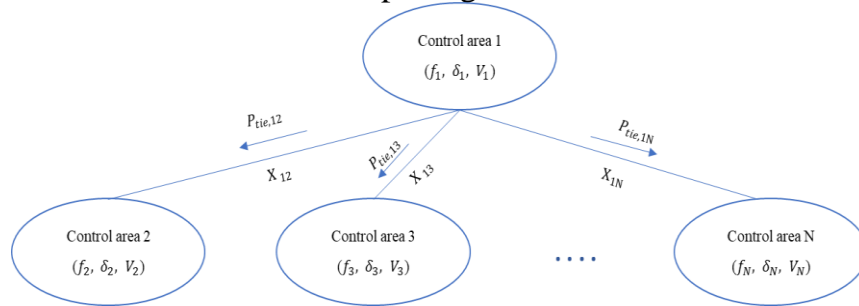


Figure 2.4. A schematic diagram of an N-area interconnected PS.

To account for the diverse dynamics of power generation and the varying levels of involvement in secondary control, the PS model for CA i is depicted in Figure 2.5.

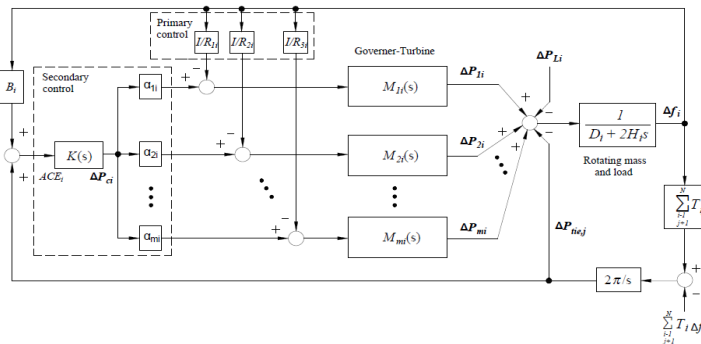


Figure 2.5. LFC system with various contributing elements and generating units in the region i

In contemporary PN, ensuring frequency stability is a crucial concern,

especially in large-scale PS that involve communication delays. In this study, Figure 2.6 depicts the component blocks schematic for the i^{th} area within the large-scale PS accounting for communication delays (Pradhan, S. K., & Das, D. K., 2020) (Fu, C., Wang, C., & Shi, D., 2020).

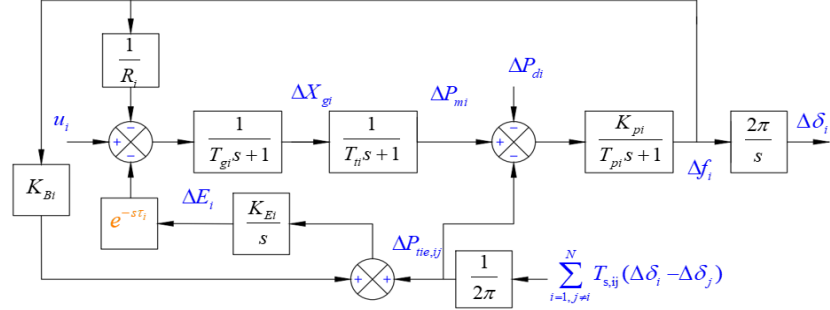


Figure 2.6. The configuration of the i^{th} area within the of the large-scale PS.

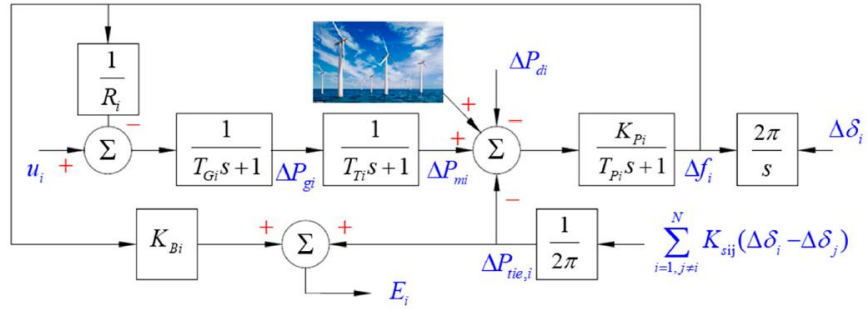


Figure 2.7. Schematic block diagram sketch for i^{th} area network, including a wind farm.

Moreover, to assess the PS's behavior when subjected to the new algorithm, we introduce the proportion of wind energy in PS is on the rise that wind speed chart is displayed in Figures 2.7. However, the inherent fluctuations in renewable energy sources and variations in load can pose challenges for LFC. In this case, the wind power generation model is added to the PS. Both wind power generation model output power and load are uncertain.

2.3. LFC-based different power system models.

In the realm of PS, LFC plays a critical role in ensuring that customers receive an adequate and dependable supply of electrical power. This chapter provides an extensive and current literature review on LFC within PS. The survey primarily focuses on LFC models designed for conventional PS, given their prominence in the field. However, the research also delves into recent advancements in LFC methodologies, addressing the unique aspects of modern PS, including deregulated PS, smart grids, microgrids, and PS integrated with renewable energy sources. Furthermore, this chapter offers a concise discussion of various control strategies. Finally, it reviews multiple control approaches applied to LFC in diverse PS such as Centralized control approach, Decentralized control approach, Categories of LFC

based on different control strategies: Classical control methods, Optimal and sub-optimal control, Adaptive control for LFC power network, Robust control, Artificial intelligence schemes, sliding mode control approach, and others Each approach's benefits and possible drawbacks are extensively examined. Notably, the review highlights that LFC based on a decentralized scheme, utilizing soft computing techniques in conjunction with renewable energy resources, is a widely researched area that still requires further refinement, given its prevalence in modern PS.

2.4. Summary

In conclusion, this extensive literature review highlights a notable research gap in the realm of LFC systems, particularly in the application of soft computing techniques. Remarkably, no prior attempts have been documented in utilizing various schemes of SMC for the design of secondary frequency control in PS. The demonstrated effectiveness and superiority of various novel SMC as an optimization tool in diverse fields has prompted the author to explore this potent optimization techniques. In pursuit of the highest dynamic performance, various innovative SMC schemes were employed for optimization. a) To formulate and implement the novel control strategies referred to as second-order integral sliding mode control (SOISMC) in the studied multi-area power models for LFC. b) To accomplish an innovative design and utilization of a single-phase sliding mode control-based state observer (SPSMCBSO) for the purpose of LFC in the context of a two-area gas-hydro-thermal power system. c) To put into practice a novel LFC approach tailored for a MASHPS under parameter uncertainty and various conditions. The proposed technique employs a second order SMC with double integrated sliding surfaces (SOSDISS), aiming to enhance frequency regulation, tie-line power management, and overall system reliability of the MASHPS.

CHAPTER 3: DESIGN OF A NEW SECOND ORDER SLIDING MODE CONTROL FOR POWER SYSTEM LOAD FREQUENCY CONTROL

In this chapter, the chattering issue poses a significant risk to actuators utilized in PS. The suggested second-order integral sliding mode control (SOISM) not only effectively mitigates chattering in control input but also enhances the robustness of the multi-area PN, making it more resilient to parametric uncertainties, including load variations and parameter mismatches. A novel LMI technique is developed to ensure the overall system's stability through the application of Lyapunov theory. Additionally, the numerical simulation studies show that the suggested controller is effective to maintain high-quality effectiveness under a variety of operational situations. This robustness is particularly valuable in the existence of fluctuating loads and matched or unmatched parameter uncertainties, among other parametric uncertainties where it effectively mitigates the high parameter uncertainties and the load disturbances, time-delay.

3.1. Formulation of a mathematical model for interconnected multi-area PS.

In this part, the suggested LFC control law is tailored for an interconnected multi-area PS, as illustrated in Figure 3.1 (Jianping, 2019) (Le, N. M. B.; Van, V. H.; Nguyen, T. M.; Tsai, Y. W. , 2018).

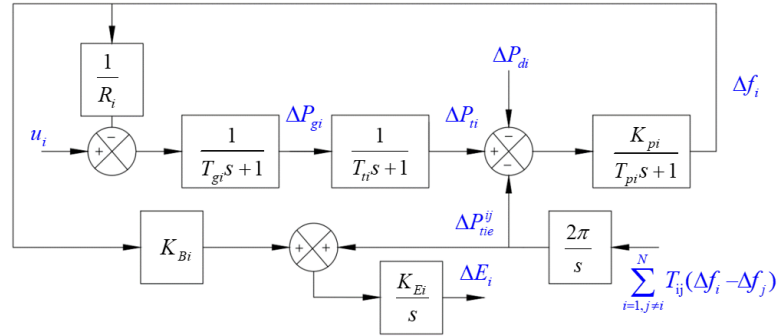


Figure 3.1. The simplified block diagram depicting the i^{th} area within a multi-area PS.

Hence, the state-space representation of the i^{th} area in matrix form in (Huynh, Van Van, Phong Thanh Tran, Bui Le Ngoc Minh, Anh Tuan Tran, Dao Huy Tuan, Tam Minh Nguyen, and Phan-Tu Vu., 2020), as depicted in the dynamic equations from (3.1) to (3.5), can be expressed as follows (3.6):

$$\dot{x}_i(t) = A_{Ti}x_i(t) + B_{Ti}u_i(t) + \sum_{\substack{j=1 \\ j \neq i}}^N H_{Tij}x_j(t) + F_{Ti}\Delta P_{Tdi}(t) \quad (3.6)$$

$$\text{where, } x_i(t) = \left[\Delta f_i(t) \quad \Delta P_{ii}(t) \quad \Delta P_{gi}(t) \quad \Delta E_i(t) \quad \Delta P_{tie}^{ij}(t) \right]^T$$

In practical PS, the operational state constantly fluctuates due to load disturbances and variations in available resources. When considering uncertainties and variations in parameters, the PS model can be described as follows:

$$\begin{aligned} \dot{x}_i(t) = & [A_{T_i} + \Theta_i(x_i, t)]x_i(t) + B_{T_i}[u_i(t) + \xi_i(x_i, t)] \\ & + \sum_{\substack{j=1 \\ j \neq i}}^N [H_{T_{ij}} + \Xi_{ij}(x_j, t)]x_j(t) + F_{T_i}\Delta P_{T_{di}}(t) \end{aligned} \quad (3.7)$$

Whereas $\Theta_i(x_i, t)$ refers to time-varying parameter uncertainties within the state matrix, $\Xi_{ij}(x_j, t)$ refers to the uncertainty in the linked matrix's time-varying parameters, and $\xi_i(x_i, t)$ is the disturbance control input. Additionally, we can refer to the combined uncertainties, with the number of areas ranging from 1 to N:

$$\bar{L}_{T_i}(x_i, t) = \Theta_i(x_i, t)x_i(t) + B_{T_i}\xi_i(x_i, t) + \sum_{\substack{j=1 \\ j \neq i}}^N \Xi_{ij}(x_j, t)x_j(t) + F_{T_i}\Delta P_{T_{di}}(t) \quad (3.8)$$

Therefore, the dynamic model (3.6) can also be expressed as:

$$\dot{x}_i(t) = A_{T_i}x_i(t) + B_{T_i}u_i(t) + \sum_{\substack{j=1 \\ j \neq i}}^N H_{T_{ij}}x_j(t) + \bar{L}_{T_i}(x_i, t) \quad (3.9)$$

In this context, the term aggregated disturbance $\bar{L}_{T_i}(x_i, t)$ encompasses uncertainties, comprising both the matched and mismatched components.

3.2. Introduction of a novel second order sliding mode load frequency control design

3.3.1. Introduction of LFC approach

In this part, we present a new approach called SOISM to address power networks facing challenges like parametric uncertainties and disturbances. Subsequently, we introduce the design of the second order SMC law, relying on the Lyapunov stability theorem. This design showcases that the system's states converge to the sliding manifold and remain on it even in the presence of uncertainty in internal parameters and external disruptions.

3.3.2. A scheme design of second order sliding LFC

Within this part, to address these challenges, we systematically outline a step-by-step process for designing and implementing this innovative controller approach.

3.4.2.1 The integral sliding surface in the context of SMC.

To elaborate further, we initiate the process by precisely developing and building an integrating sliding surface designed for MAPS (3.9)

$$\sigma_{T_i}[x_i(t)] = G_{T_i}x_i(t) - \int_0^t G_{T_i}(A_{T_i} - B_{T_i}K_{T_i})x_i(\tau)d\tau \quad (3.11)$$

where G_{T_i} is a continuous matrix and K_{T_i} is the matrix of design, matrix G_{T_i} is selected to ensure that matrix $G_{T_i}B_{T_i}$ is nonsingular. The matrix of design

$K_{T_i} \in R^{m_i \times n_i}$ chosen in such a way that it satisfies the inequality condition of the PS.
 $\text{Re}[\lambda_{\max}(A_{T_i} - B_{T_i}K_i)] < 0$ (3.12)

When we combine (3.9) with the ability to identify and distinguish $\sigma_{T_i}[x_i(t)]$ regarding time, then.

$$\begin{aligned} \dot{\sigma}_{T_i}[x_i(t)] = & G_{T_i}[A_{T_i}x_i(t) + B_{T_i}u_i(t) + \sum_{\substack{j=1 \\ j \neq i}}^N H_{T_{ij}}x_j(t) + \bar{L}_{T_i}(x_i, t) \\ & - G_{T_i}(A_{T_i} - B_{T_i}K_i)x_i(t) \end{aligned} \quad (3.13)$$

Therefore, the configuration $\sigma_{T_i}[x_i(t)] = \dot{\sigma}_{T_i}[x_i(t)] = 0$, the equivalent control can be expressed as

$$\begin{aligned} u_i^{eq}(t) = & -(G_{T_i}B_{T_i})^{-1}[G_{T_i}A_{T_i}x_i(t) + \sum_{\substack{j=1 \\ j \neq i}}^N G_{T_i}H_{T_{ij}}x_j(t) + G_{T_i}\bar{L}_{T_i}(x_i, t) \\ & - G_{T_i}(A_{T_i} - B_{T_i}K_{T_i})x_i(t)] \end{aligned} \quad (3.14)$$

Alternating $u_i(t)$ with $u_i^{eq}(t)$ into the PS (3.9) gives the movement of sliding.

$$\begin{aligned} \dot{x}_i(t) = & (A_{T_i} - B_{T_i}K_{T_i})x_i(t) + [I_i - B_{T_i}(G_{T_i}B_{T_i})^{-1}G_{T_i}]\bar{L}_{T_i}(x_i, t) \\ & + \sum_{\substack{j=1 \\ j \neq i}}^N [I_i - B_{T_i}(G_{T_i}B_{T_i})^{-1}G_{T_i}]H_{T_{ij}}x_j(t) \end{aligned} \quad (3.15)$$

The subsequent theorem establishes a condition under which the second order sliding mode dynamic Equation (3.15) demonstrates asymptotic stability.

3.3.2.2 Analysis of the MAPS's stability in sliding mode dynamics

Theorem 3.1. The sliding motion (3.15) is only asymptotically stable when a symmetric positive definite matrix is included $P_i, i = 1, 2, \dots, N$, and positive scalars $\hat{\epsilon}_i$ and α_j as a result of which the subsequent LMIs are obtained.

$$\begin{bmatrix} (A_{T_i} - B_{T_i}K_{T_i})^T P_i + P_i(A_{T_i} - B_{T_i}K_{T_i}) + \sum_{\substack{j=1 \\ j \neq i}}^N \alpha_j^{-1} H_{T_{ji}}^T H_{T_{ji}} & P_i[I_i - B_{T_i}(G_{T_i}B_{T_i})^{-1}G_{T_i}] \\ [I_i - B_{T_i}(G_{T_i}B_{T_i})^{-1}G_{T_i}]^T P_i & -\hat{\epsilon}_i^{-1} \end{bmatrix} < 0 \quad (3.16)$$

3.3.3. Load frequency control design

In the subsequent step, we introduce a novel SOISMIC scheme for MAPS. This scheme is designed to mitigate the issues of chattering and oscillations associated with the ISS. The sliding manifold is defined and established in the following way $S_{T_i}[x_i(t)]$ as

$$\bar{S}_{T_i}[x_i(t)] = \dot{\sigma}_{T_i}[x_i(t)] + \delta_i \sigma_{T_i}[x_i(t)] \quad (3.17)$$

and

$$\dot{\bar{S}}_{Ti}[x_i(t)] = \ddot{\sigma}_{Ti}[x_i(t)] + \delta_i \dot{\sigma}_{Ti}[x_i(t)] \quad (3.18)$$

where $\delta_i > 0$ is a positive constant. Referring to equation (3.9), equation (3.18) can be expressed as

$$\begin{aligned} \dot{\bar{S}}_{Ti}[x_i(t)] = & G_i[A_{Ti}\dot{x}_i(t) + B_{Ti}\dot{u}_i(t) + \sum_{\substack{j=1 \\ j \neq i}}^N H_{Tij}\dot{x}_j(t) + \dot{\bar{L}}_{Ti}(x_i, t)] \\ & - G_{Ti}(A_{Ti} - B_{Ti}K_{Ti})\dot{x}_i(t) + \delta_i \dot{\sigma}_{Ti}[x_i(t)] \end{aligned} \quad (3.19)$$

Building upon the definitions of the sliding surface and the sliding manifold, we can formulate the continuous decentralized second order sliding mode LFC for PN as follows:

$$\begin{aligned} \dot{u}_i(t) = & -(G_{Ti}B_{Ti})^{-1}[\|G_{Ti}\| \|B_{Ti}\| \|K_{Ti}\| \|\dot{x}_i(t)\| + \sum_{\substack{j=1 \\ j \neq i}}^N \|G_{Tj}\| \|H_{Tji}\| \|\dot{x}_j(t)\| + \delta_i \|\dot{\sigma}_{Ti}[x_i(t)]\| \\ & + \|G_{Ti}\| \|\bar{\gamma}_i + \bar{\varepsilon}\| \frac{\bar{S}_{Ti}[x_i(t)]}{\|\bar{S}_{Ti}[x_i(t)]\|} \end{aligned} \quad (3.20)$$

3.3. Simulation results and discussions

3.3.1. Frequency control in practical power system

In practical PS, by doing so, we aim to enhance the performance of the PS, primarily by mitigating chattering in comparison to employing the same SMC technique. This evaluation is conducted on a two-area interconnected PS, as depicted in Figure 3.2.

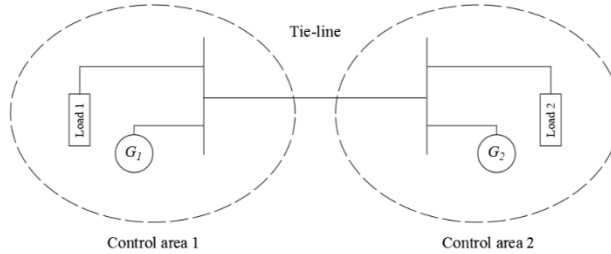


Figure 3.2. The simplified block diagram illustrates the connection between control areas 1 and 2.

3.3.2. Various cases of simulation results

In a power plant, to accomplish the system's nominal terms frequency (typically 50 Hz) and designed power interchange with surrounding systems, the AGC balances total generating and loading (including losses). The reporting of various simulations is examined with their various operating circumstances outlined below:

3.3.2.1. LFC the proposed second order sliding mode controller

In this study, we examine a standard two-area conventional PN in Figure 3.3. The purpose is to assess and analyze the proposed controller within this system,

demonstrating its strength and efficiency, as outlined for the SOISMCM.

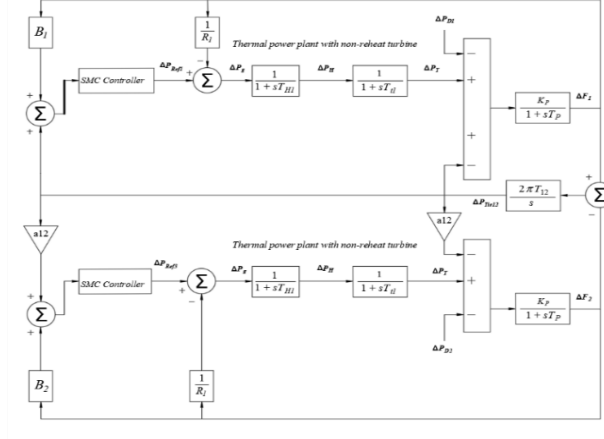


Figure 3.3. Transfer function model of multi area thermal system with SMC controller.

Simulation 1:

In this section, three different scenarios or cases are investigated. The PS parameters for the two-area PN are provided in the previous section (Guo, J., 2019).

Case 1. To proceed, let's once again assume that the system is operating with nominal parameters. Load disturbances are introduced into the system at $\Delta P_{d1} = 0.01$ seconds for area 1 at $t_1 = 1$ s and $\Delta P_{d2} = 0.02$ seconds for area 2 at $t = 1$ s within the PN. As illustrated in Figure 3.4 (a), the frequency deviation signals for control area 1 and 2 are shown.

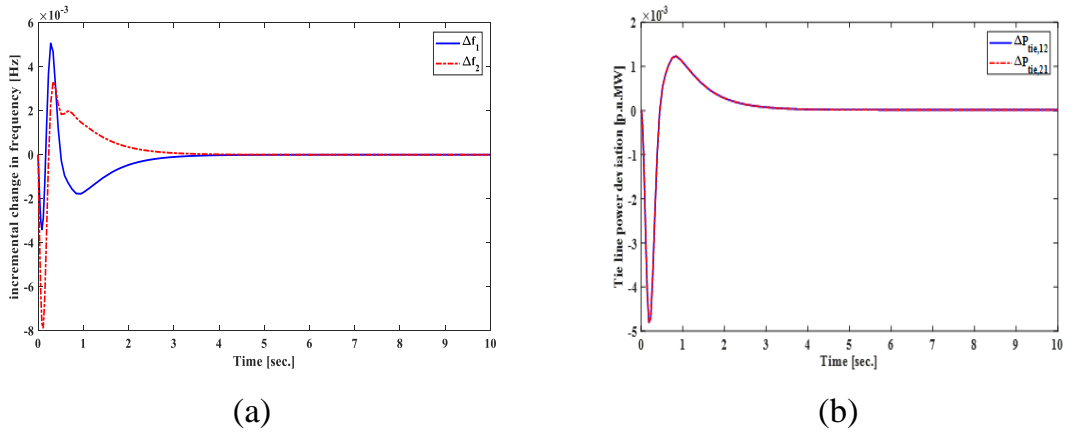


Figure 3.4. Frequency variation [Hz] (a) and Tie-line power variation [p.u.MW] (b) of both control areas with matched disturbances.

Figure 3.4 (b) presents the tie-line power flow signals for each area. With novel control scheme, these results emphasize the PS's swift and effective transient response in mitigating and eliminating the chattering issue. It is readily apparent that the frequency errors, the tie-line power errors, and CA errors all converge to zero

within a short timeframe, in stark contrast to previous control methodologies outlined in (Guo, J., 2019).

Remark 3.1. Depending on the range of frequency variation, different FCL may be necessary to maintain PS frequency stability. Without controllers in place for the PS, significant frequency deviations can lead to various issues, including equipment damage, degraded load performance, transmission line overloads, and interference with system protection schemes. Ultimately, this can result in an unstable condition for the PS. Hence, the presence of frequency controllers is essential for PS operation.

Case 2. In the previous scenarios, to further investigate its robustness under different conditions, we introduced $\pm 20\%$ deviations from the nominal parameters and applied load disturbances. This allowed us to assess the robustness and efficacy of the novel SOISM scheme. Figure 3.5 (c) illustrates the frequency deviation of generators, highlighting that the suggested second order scheme enables the PS to return to its nominal value within approximately 5–6 seconds after experiencing load disturbances. The scheduled values of tie-line power deviations are depicted in Figure 3.5 (d).

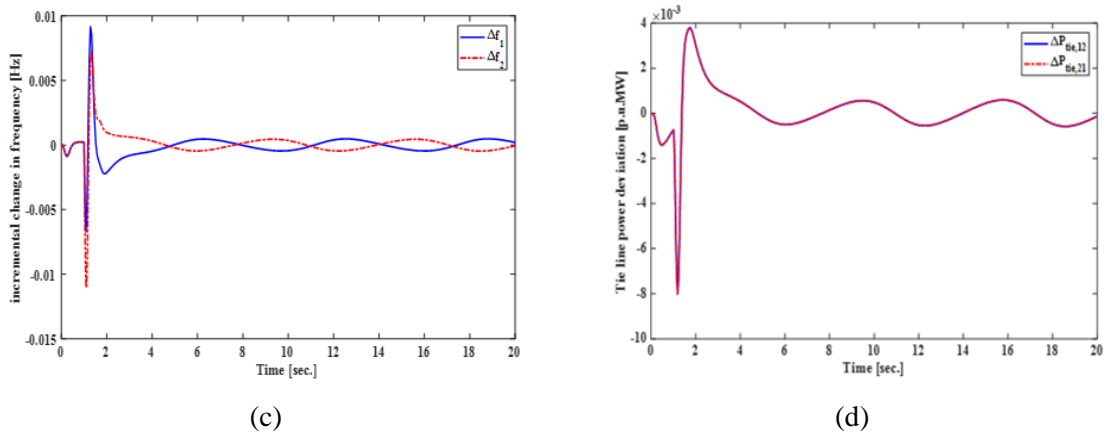


Figure 3.5. Frequency [Hz] (c) and Tie-line power [p.u.MW] (d) both control areas under unmatched disturbances.

Remark 3.2. By implementing the second-order control law, it becomes feasible to achieve shorter settling times, smaller transient deviations, and reduced oscillations when dealing with load disturbances. This approach effectively resolves some limitations observed in other control strategies presented in the paper by (Guo, J., 2019), particularly in terms of decreasing chattering effects and enhancing transient response.

Case 3. In the final case, we examine the impact of load deviations and unmatched parameter uncertainties in a two-area PS. To demonstrate the advantages of the suggested SOISM scheme, random load deviations are applied to the two-area PN in Figure 3.6.

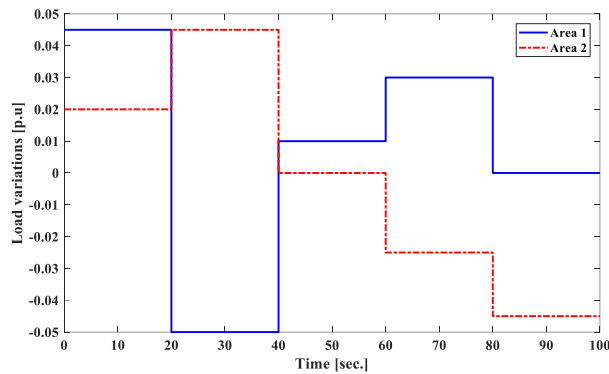


Figure 3.6. Deviation load of both areas of the PS.

The simulation results, displayed in Figures 3.7 (e) to 3.7 (f), showcase the frequency deviation, tie-line power, providing a clear representation of performance under different scenarios involving load deviations and unmatched parameter uncertainties.

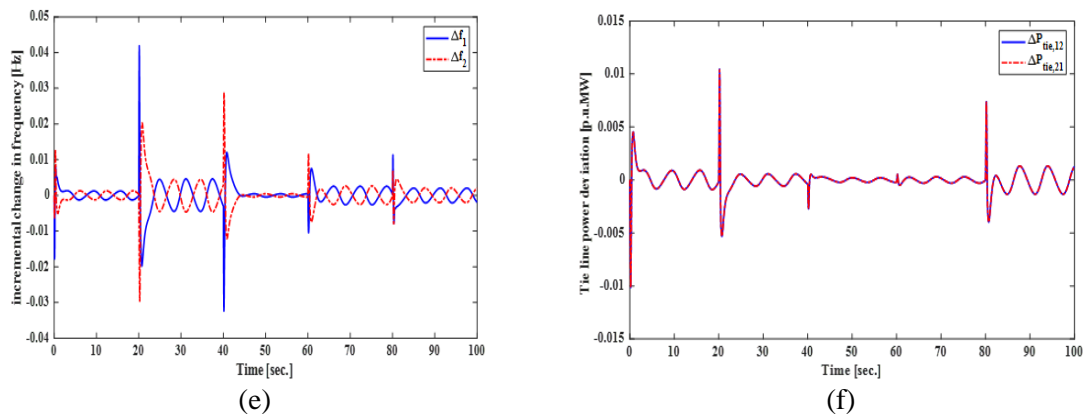


Figure 3.7. Change of frequency [Hz] and Tie-line power [p.u.MW] underload deviations and the unmatched uncertainty in the parameters.

Simulation 2: In contemporary PN, ensuring frequency stability is a crucial concern, especially in large-scale PS that involve communication delays.

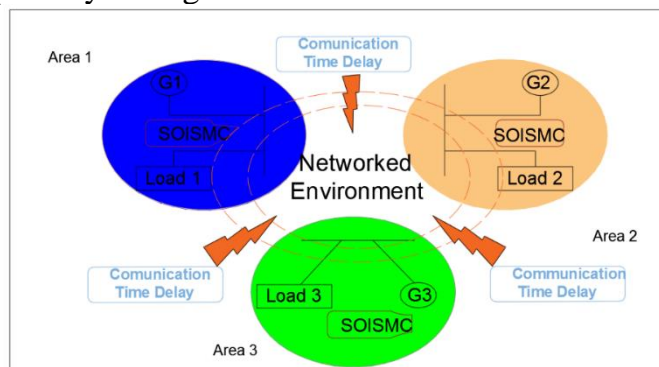


Figure 3.8. The layout of the interconnected PN with time delays.

In this study, Figure 3.8 shows the layout of the interconnected PN accounting for communication delays (Pradhan, S. K., & Das, D. K., 2020) (Fu, C., Wang, C., &

Shi, D., 2020). In diverse scenarios and under various conditions, the efficiency and resilience of the suggested SOISMIC approach using an interconnected time-delay PN. The LFC approach based on SOISMIC, as presented here, is subject to a comparative analysis with the traditional LFC approach detailed in (Sarkar, M. K., Dev, A., Asthana, P., & Narzary, D., 2018. In this specific case, load disturbances of magnitude (in per unit Megawatts) occur at time $t=0$ s in a three-area LSPS. The corresponding frequency variations for the large-scale PS, which incorporates delay times of $\tau_i = 3$ s, are illustrated in Figure 3.9 (a) to Figure 3.9 (b).

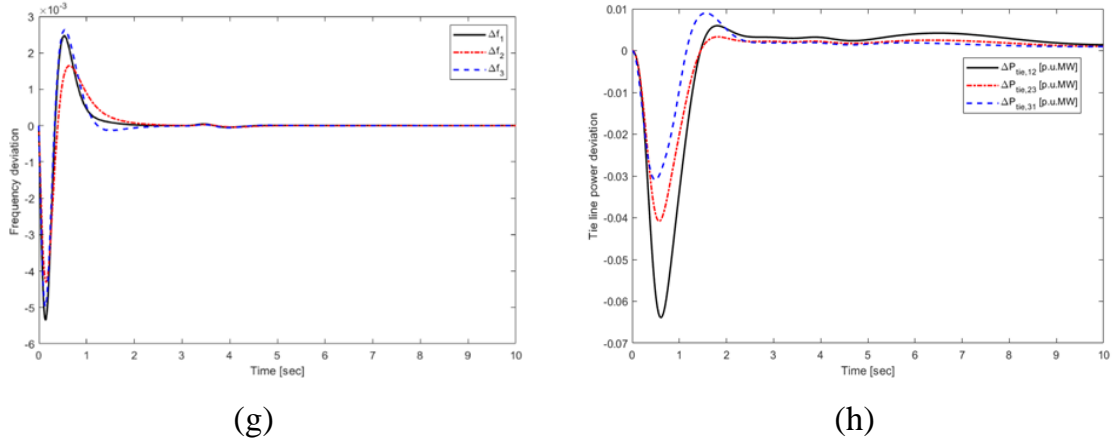


Figure 3.9. Frequency deviation of the PS (g) and Tie-line deviation of the PS. (h).

Remark 3.3: In this setup, we have considered the influence of time-delay signals for the purpose of three areas MAPS under random load disturbance. It is evident that the SOISMIC based on the provided switching surface not only achieves superior response speed but also enhances transient performance, resulting in a reduction within multi-area interconnected time-delay power grids.

3.4. Conclusion

In summary, this study introduces a novel SOISMIC scheme for effectively managing the active power balance in a MAPS. This is accomplished by prioritizing the active power balancing, minimizing excessive overshoot, and accelerating the frequency transient response with the use of an integrated sliding surface-based second order SMC. The solution of the chattering issue demonstrates the effectiveness of the MAPS and shows gains over earlier control techniques. Notably, in practical applications, the suggested SMC technique combined with the FLC approach provides a strong and efficient solution while removing chattering. By reducing chattering in the control input, the suggested control scheme supplies accurate signals to control mechanical inertia power, enabling it to effectively match load changes or demands. This capability makes it highly suitable for practical PS dealing with significant parameter uncertainties, load disturbances, communication delays in PS.

CHAPTER 4: DESIGNING AN ADVANCED SLIDING MODE OBSERVER FOR LOAD FREQUENCY CONTROL IN MULTI-AREA MULTI-SOURCE POWER SYSTEMS

In this session, the single-phase sliding mode control-based state observer (SPSMCBSO) is used to introduce the LFC of the two areas gas-hydro-thermal power system (TAGHTPS). Second, the state variables for feedback control are estimated using the state observer. Third, the SPSMCBSO is designed to alter the fundamental SMC to enhance TAGHTPS performance with respect to overshoot and settling time. Furthermore, to resolve the challenge of measuring the state variable, the SPSMCBSO is designed to completely rely on the state observer. Fourth, a novel LMI scheme-Lyapunov stabilization hypothesis has been applied to carry out the TAGHTPS stability study. The experiment's outcomes are presented and compared against reputable traditional control techniques, the SPSMCBSO further demonstrated robustness and is not affected by subsystem parameter deviation, random load disturbance, and parameter uncertainty in state and interconnected matrix, the inherent fluctuations in renewable energy sources.

4.1. Mathematical model of the interconnected multi-area multi-source PS

This portion includes, as a result, as seen in Figure 4.1, we take TAGHTPS into account in each region in this section. The i^{th} region of the PS state space in the model is obtained by specifying the PS parameters and applying the dynamics expression from (4.1) to (4.13) (Huynh, V. V., Tran, P. T., Nguyen, T. M., Phan, V. D., & Pham, V. T., 2022), which is provided by (4.14).

$$\dot{x}_i(t) = A_{Ti}x_i(t) + B_{Ti}u_i(t) + \sum_{\substack{j=1 \\ j \neq i}}^L H_{Tij} + \Delta H_{Tij}x_j(t) + F_{Ti}\Delta P_{Tdi}(t) \quad (4.14)$$

where the state space structure of the TAGHTPS is represented by formula (4.14)

$x_i(t) = \left[\Delta f_i \quad \Delta P_{pt_i} \quad \Delta P_{Gt_i} \quad \Delta X_{Et_i} \quad \Delta P_{Gh_i} \quad \Delta P_{Rh_i} \quad \Delta X_{Eh_i} \right. \\ \left. \Delta P_{Gg_i} \quad \Delta P_{Rg_i} \quad \Delta P_{Vg_i} \quad \Delta X_{Eg_i} \quad \Delta ACE_i \quad \Delta P_{tie_{ij}} \right]^T$ is the vector of states, $x_j(t)$ is the system's state vector of the linked system of $x_i(t)$, $u_i(t)$ is the vector of control, and $\Delta P_{di}(t)$ is the disturbance. A_{Ti} , B_{Ti} , H_{Tij} and F_{Ti} are the system matrices.

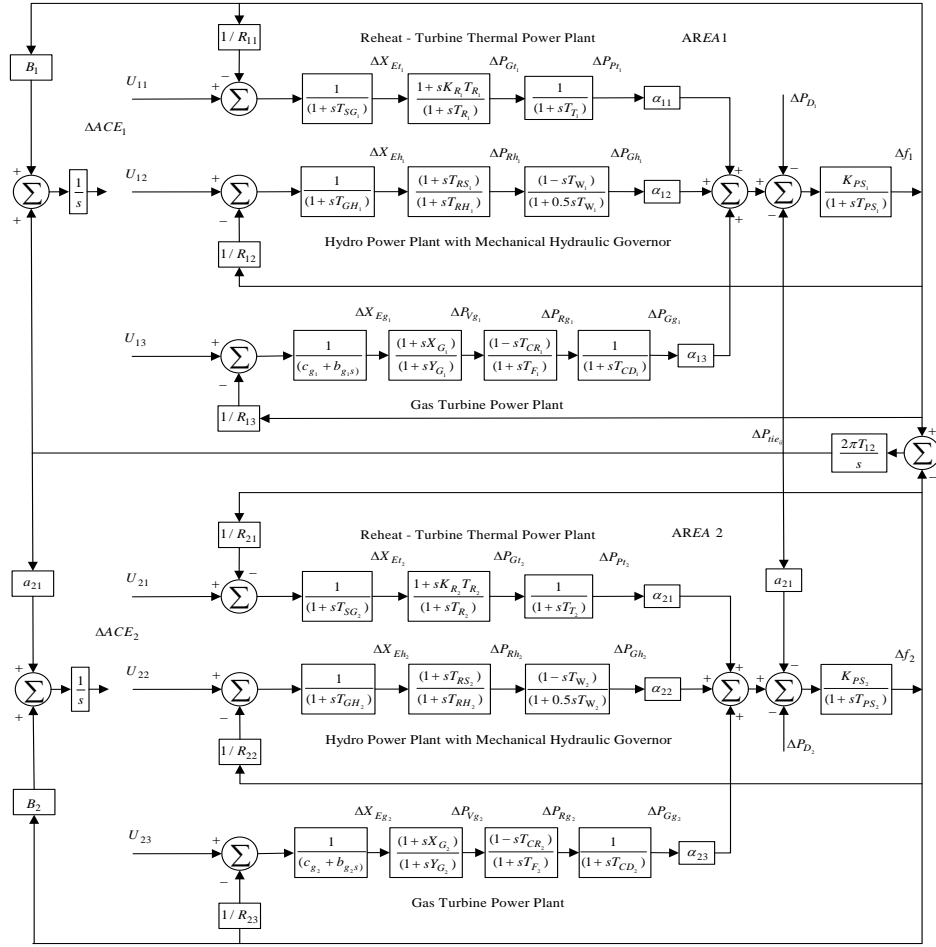


Figure 4.1. Schematic of TAMSPS's LFC blocks.

In the practical MAMSPS, variations in operating conditions continually impact the dynamic load sources. Taking this factor into account, equation (4.14) can be reformulated as follows:

$$\begin{aligned} \dot{x}_i(t) = & [A_{Ti} + \Sigma_i(x_i, t)]x_i(t) + B_{Ti}[u_i(t) + \psi_i(x_i, t)] \\ & + \sum_{\substack{j=1 \\ j \neq i}}^L [H_{Tij} + \Xi_{ij}(x_j, t)]x_j(t) + F_{Ti}\Delta P_{Tdi}(t) \end{aligned} \quad (4.15)$$

where $\Sigma_i(x_i, t)$, $\Xi_{ij}(x_j, t)$ are uncertainty caused by time-varying parameters and $B_{Ti}\psi_i(x_i, t)$ is the input disturbance. To put it differently, the total uncertainty can be expressed as:

$$\Phi_i(x_i, t) = \Sigma_i(x_i, t)x_i(t) + B_{Ti}\psi_i(x_i, t) + \sum_{\substack{j=1 \\ j \neq i}}^L \Xi_{ij}x_j(t) + F_{Ti}\Delta P_{Tdi}(t) \quad (4.16)$$

Hence, the updated dynamic model can be represented as:

$$\dot{x}_i(t) = A_{T_i}x_i(t) + B_{T_i}u_i(t) + \sum_{\substack{j=1 \\ j \neq i}}^L H_{T_{ij}}x_j(t) + \Phi_i(x_i, t) \quad (4.17)$$

$$y_i = C_{T_i}x_i$$

where $\Phi_i(x_i, t)$ expresses the uncertainty of the matched and unmatched parameters as a combined disturbance.

4.2. Designing the power system state estimator

In the case of PS, when some state variables are difficult to address, few publications have used observer approaches to solve the LFC. Because of the above, we use the observer approach to recreate the original TAGHTPS (4.17) framework in the manner shown below.

$$\dot{\hat{x}}_i(t) = A_{T_i}\hat{x}_i(t) + B_{T_i}u_i(t) + \sum_{\substack{j=1 \\ j \neq i}}^L H_{T_{ij}}\hat{x}_j(t) + \Gamma_{T_i}(y_i - \hat{y}_i) \quad (4.18)$$

$$\hat{y}_i = C_{T_i}\hat{x}_i$$

where Γ_{T_i} is the observer gain, $\hat{x}_i(t)$ is the estimation of $x_i(t)$, y_i is the output vector, \hat{y}_i is the result of the state observer, correspondingly. With the pole positioning approach, it may be computed. The state error changing is then examined, and the state error is reported as

$$\tilde{x}_i(t) = x_i(t) - \hat{x}_i(t) \quad (4.19)$$

Differentiating the error \tilde{x}_i we get

$$\dot{\tilde{x}}_i = (A_{T_i} - \Gamma_{T_i}C_{T_i})\tilde{x}_i + \sum_{\substack{j=1 \\ j \neq i}}^L H_{T_{ij}}\tilde{x}_j + \Phi_i(x_i, t) \quad (4.20)$$

The convergence of the state error towards zero depends on the eigenvalues of $(A_{T_i} - \Gamma_{T_i}C_{T_i})$

4.3. Design of the PS state estimator

In practical scenarios, the LFC scheme needs to exhibit a high level of robustness against specific disturbances to ensure the stability of MAMSPS. To address this, we introduce the SPSMCBSO along with a sliding surface that does not require a reaching phase, defined as follows:

$$\eta_{T_i}[\hat{x}_i(t)] = M_{T_i}\hat{x}_i(t) - \int_0^t M_{T_i}(A_{T_i} - B_{T_i}\Lambda_{T_i})\hat{x}_i(\tau)d\tau - M_{T_i}\hat{x}_i(0)e^{-\delta t} \quad (4.21)$$

where M_{T_i} is chosen to guarantee that the matrix $M_{T_i}B_{T_i}$ is nonsingular. The design matrix $\Lambda_{T_i} \in R^{m_i \times n_i}$ is selected to meet the non-linearity requirement.

$$\text{Re}[\lambda_{\max}(A_{T_i} - B_{T_i}\Lambda_{T_i})] < 0 \quad (4.22)$$

if we take derivative of $\eta_{T_i}[\hat{x}_i(t)]$ in terms of time, we've got the items that

follow.

$$\begin{aligned} \dot{\eta}_{T_i} [\hat{x}_i(t)] = & [M_{T_i} A_{T_i} \hat{x}_i(t) + M_{T_i} B_{T_i} u_i(t) + \sum_{\substack{j=1 \\ j \neq i}}^L M_{T_i} H_{T_{ij}} \hat{x}_j(t) + M_{T_i} \Gamma_{T_i} (y_i - \hat{y}_i)] \\ & - M_i (A_{T_i} - B_{T_i} \Lambda_{T_i}) \hat{x}_i(t) + \delta_i M_{T_i} \hat{x}_i(0) e^{-\delta_i t} \end{aligned} \quad (4.23)$$

As $\dot{\eta}_{T_i}(t) = \eta_{T_i}(t) = 0$, then we can express the equivalent control a

$$\begin{aligned} u_i^{eq}(t) = & -(M_{T_i} B_{T_i})^{-1} [M_{T_i} A_{T_i} \hat{x}_i(t) + \sum_{\substack{j=1 \\ j \neq i}}^L M_{T_i} H_{T_{ij}} \hat{x}_j(t) + M_{T_i} \Gamma_{T_i} (y_i - \hat{y}_i) \\ & - M_{T_i} (A_{T_i} - B_{T_i} \Lambda_{T_i}) \hat{x}_i(t) + \delta_i M_{T_i} \hat{x}_i(0) e^{-\delta_i t}] \\ = & -(M_{T_i} B_{T_i})^{-1} [M_{T_i} B_{T_i} \Lambda_{T_i} \hat{x}_i(t) + M_{T_i} \Gamma_{T_i} (y_i - \hat{y}_i) + \delta_i M_{T_i} \hat{x}_i(0) e^{-\delta_i t} \\ & + \sum_{\substack{j=1 \\ j \neq i}}^L M_{T_i} H_{T_{ij}} \hat{x}_j(t)] \end{aligned} \quad (4.24)$$

By completing the system's loop, we provide (4.24) into (4.17)

$$\begin{aligned} \dot{x}_i(t) = & (A_{T_i} - B_{T_i} \Lambda_{T_i}) x_i(t) + (B_{T_i} \Lambda_{T_i} - B_{T_i} (M_{T_i} B_{T_i})^{-1} M_{T_i} \Gamma_{T_i} C_{T_i}) \tilde{x}_i(t) \\ & + \sum_{\substack{j=1 \\ j \neq i}}^L [H_{T_{ij}} - B_{T_i} (M_{T_i} B_{T_i})^{-1} M_{T_i} H_{T_{ij}}] x_j(t) \\ & + \sum_{\substack{j=1 \\ j \neq i}}^L B_{T_i} (M_{T_i} B_{T_i})^{-1} M_{T_i} H_{T_{ij}} \tilde{x}_j(t) + \Phi_i(x_i, t) - \delta_i B_{T_i} (M_{T_i} B_{T_i})^{-1} M_{T_i} \hat{x}_i(0) e^{-\delta_i t} \end{aligned} \quad (4.25)$$

To examine MAMSPS (4.17), we integrate equations (4.20) and (4.25) as follows.

$$\begin{aligned} \begin{bmatrix} \dot{x}_i \\ \dot{\tilde{x}}_i \end{bmatrix} = & \begin{bmatrix} A_{T_i} - B_{T_i} \Lambda_{T_i} & \Theta_i \\ 0 & A_{T_i} - \Gamma_{T_i} C_{T_i} \end{bmatrix} \begin{bmatrix} x_i \\ \tilde{x}_i \end{bmatrix} + \sum_{\substack{j=1 \\ j \neq i}}^L \begin{bmatrix} H_{T_{ij}} - Y_i H_{T_{ij}} & Y_i H_{T_{ij}} \\ 0 & H_{T_{ij}} \end{bmatrix} \begin{bmatrix} x_j \\ \tilde{x}_j \end{bmatrix} \\ & + \begin{bmatrix} \Phi_i(x_i, t) \\ \Phi_i(x_i, t) \end{bmatrix} + \begin{bmatrix} N_i e^{-\delta_i t} \\ 0 \end{bmatrix} \end{aligned} \quad (4.26)$$

where $\Theta_i = B_{T_i} \Lambda_{T_i} - B_{T_i} (M_{T_i} B_{T_i})^{-1} M_{T_i} \Gamma_{T_i} C_{T_i}$,

$N_i = -\delta_i B_{T_i} (M_{T_i} B_{T_i})^{-1} M_{T_i} \hat{x}_i(0)$ and $Y_i = B_{T_i} (M_{T_i} B_{T_i})^{-1} M_{T_i}$.

Equation (4.25) represents the dynamic system of the MAMSPS. Therefore, we proceed to assess the stability (4.26) of this system using the novel LMI provided in (4.27), accompanied by the corresponding theorem as stated.

Theorem 4.1: Asymptotically stable is formula (4.26) provided that the symmetric definite positive matrix Π_i and $\bar{\Pi}_i$ where $i = 1, 2, \dots, L$ and the positive scalars λ_i, ρ_i and $\hat{\gamma}_i$ assuming the specified conditions, we can establish that the new LMI below holds.

$$\begin{bmatrix} X_i & \Pi_i \Theta_i & \Pi_i & \Pi_i N_i & 0 \\ \Theta_i^T \Pi_i & \bar{X}_i & 0 & 0 & \bar{\Pi}_i \\ \Pi_i & 0 & -\lambda_i^{-1} & 0 & 0 \\ N_i^T \Pi_i & 0 & 0 & -\hat{\gamma}_i^{-1} & 0 \\ 0 & \bar{\Pi}_i & 0 & 0 & -\rho_i^{-1} \end{bmatrix} < 0 \quad (4.27)$$

where $X_i = \Pi_i (A_{Ti} - B_{Ti} \Lambda_{Ti}) + (A_{Ti} - B_{Ti} \Lambda_{Ti})^T \Pi_i$

$$+ \sum_{\substack{j=1 \\ j \neq i}}^L [\bar{\lambda}_j (H_{Tji} - \Upsilon_j H_{Tji})^T (H_{Tji} - \Upsilon_j H_{Tji})],$$

$$\bar{X}_i = \bar{\Pi}_i (A_{Ti} - \Gamma_{Ti} C_{Ti}) + (A_{Ti} - \Gamma_{Ti} C_{Ti})^T \bar{\Pi}_i + \sum_{\substack{j=1 \\ j \neq i}}^L [\tilde{\lambda}_j^{-1} H_{Tji}^T H_{Tji}]$$

$$+ \sum_{\substack{j=1 \\ j \neq i}}^L [\hat{\lambda}_j (\Upsilon_j \tilde{H}_{Tji})^T \Upsilon_j \tilde{H}_{Tji}].$$

4.4. Design of a sliding mode controller with total output feedback

In this section, we develop SMC technique with single phase decentralization for LFC in the context of the MAMSPS described by Equation (4.17).

$$\begin{aligned} u_i(t) = & -(M_{Ti} B_{Ti})^{-1} [\|M_{Ti}\| \|B_{Ti}\| \|\Lambda_{Ti}\| \|\hat{x}_i(t)\| \\ & + \delta_i \|M_{Ti}\| \|\hat{x}_i(0)\| e^{-\delta_i t} + \|M_{Ti}\| \|\Gamma_{Ti}\| \|(y_i - \hat{y}_i)\| \\ & + \sum_{\substack{j=1 \\ j \neq i}}^L [\|M_{Tj}\| \|H_{Tji}\| \|\hat{x}_i(t)\| + \theta_i] \frac{\eta_{Ti}[\hat{x}_i(t)]}{\|\eta_{Ti}[\hat{x}_i(t)]\|}, \end{aligned} \quad (4.28)$$

$$i = 1, 2, \dots, L$$

where θ_i is the positive scalar and $u_i(t)$ represents the decentralized single phase SMC approach. In this subsection, we also derive proof of the system state variables' reachability, along with the Lyapunov function associated with the following theorem. Following that, Figure 2 depicts the flowchart of the proposed observer single-phase sliding mode control technique.

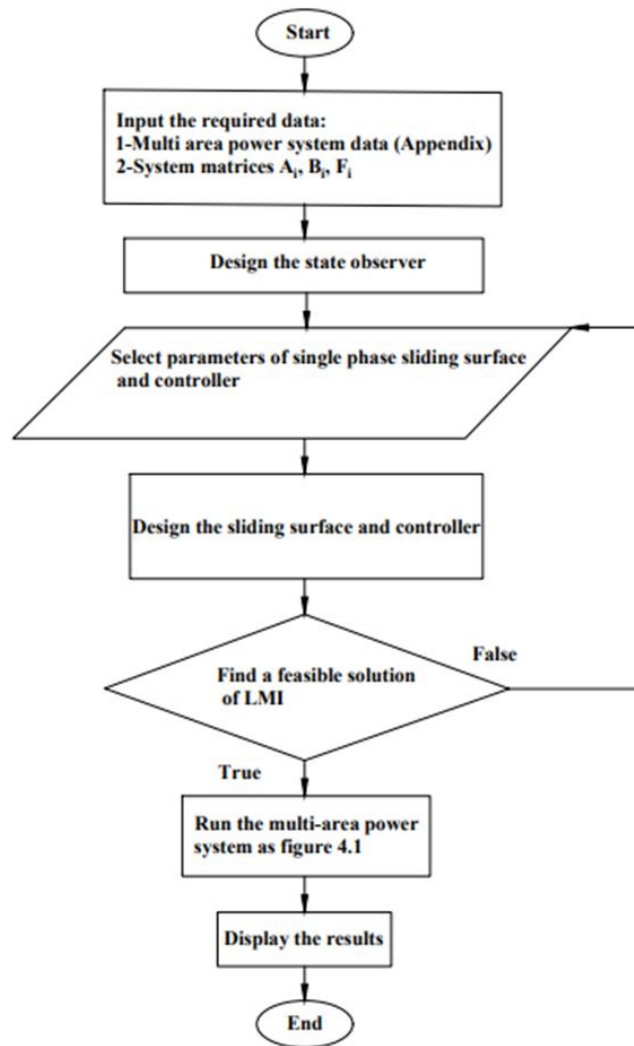


Figure 4.2. The visual representation depicting the SPSMCBSO approach as a flowchart.

Remark 4.1. The fundamental function of a single-phase SMC is to provide motion strength over the whole state space. In the sliding mode, the size of the state space is according to the order of the motion equation. As such, the resilience of intricately linked PS may be guaranteed over the duration of the system's reaction, beginning at the first-time instance.

4.5. Simulation results and discussions

In the presence of random and step load disturbances as well as parameter uncertainties, the efficiency of the suggested SPSMCBSO for the LFC of the TAGHTPS is demonstrated in three simulations in the present session, which tests the effectiveness and resilience of the suggested control approach.

4.5.1 Simulation 1

Case 1: Utilizing the subsystem parameter from (G. Nidhi, K. Narendra, B. Chitti, 2019) and a step load disturbance of 1%, the TAGHTPS response was once

more simulated using the Jaya approach to create PID structured regulators for the Optimized Generation Control approach. Using the suggested method, we mimic the TAGHTPS response in this instance, using conditions akin to those reported in (G. Nidhi, K. Narendra, B. Chitti., 2019) .

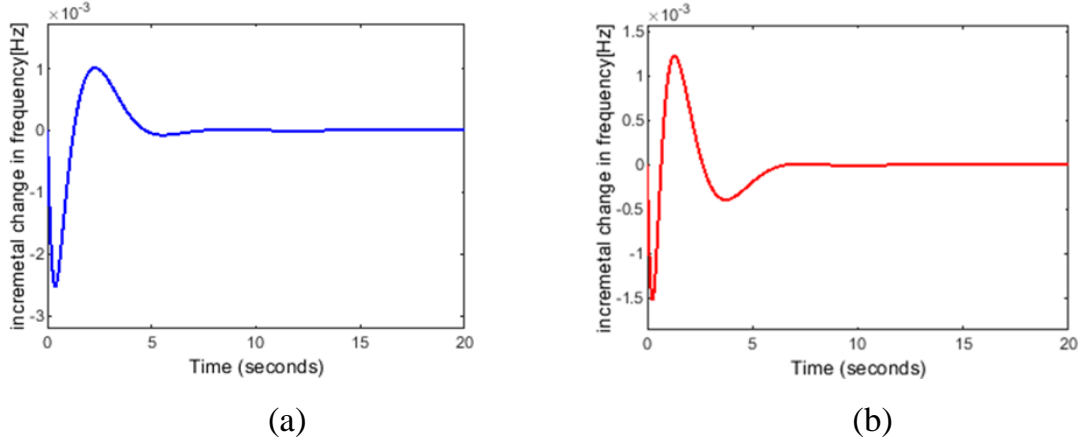


Figure 4.3. Frequency variation [Hz] in area 1 (a) and area 2 (b).

In Figure 4.3 (a), the frequency fluctuation of area one is shown. In Figure 4.3 (b), the FD in area two is displayed. Figure 4.4 provides the tie line power , in that order.

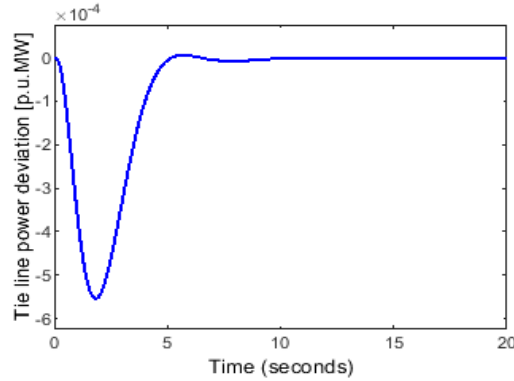


Figure 4.4. Tie line power variation [p.u.MW]

Better overshoot is observed for both controllers; nevertheless, the 5 s settling time with the suggested method is once more much less than the 8 s settling duration with the controller described in (G. Nidhi, K. Narendra, B. Chitti., 2019). This further suggests that the simpler and less demanding way to execute the recommended system is a better choice for the MAMSPS LFC.

Case 2: In this case, our simulation involves subjecting the TAGHTPS to a response analysis in the presence of random load disturbances, as depicted in Figure 4.8 with $\pm 20\%$ deviation in the subsystem parameters. Moreover, we account for mismatched uncertainties in the system state matrix due to changes in valve positions within the TAGHTPS. These uncertainties are represented by a cosine function, which adds another layer of complexity to the analysis.

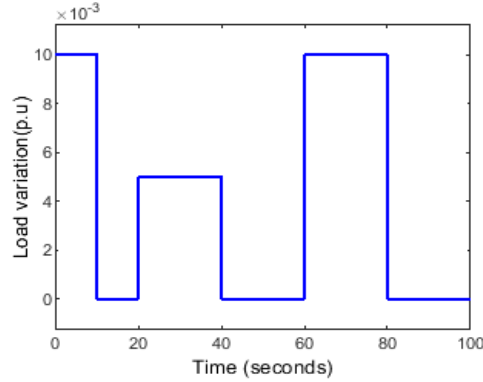


Figure 4.5. Deviation in random load.

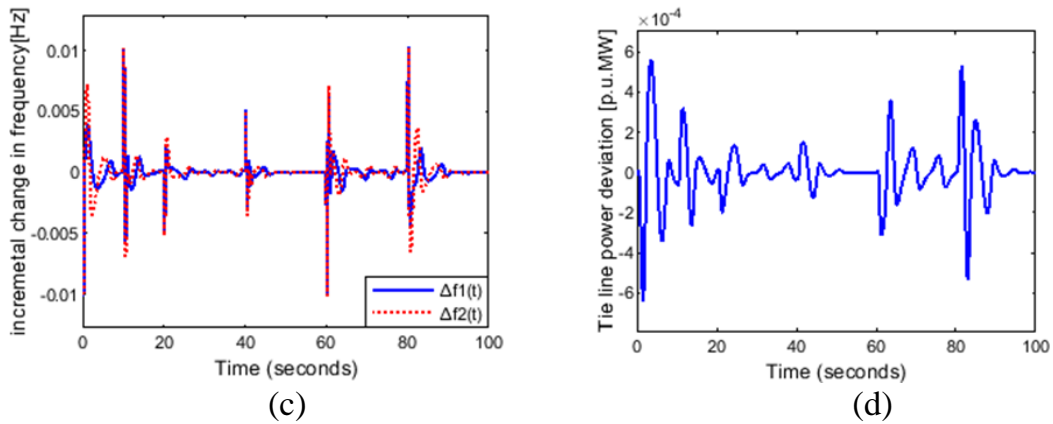


Figure 4.6. Frequency variations [Hz] (e) and Changes in tie line power [p.u.MW] (f) in area-1 and area-2.

Figure 4.6 (c) shows the frequency variation in both locations, while Figure 4.6 (d) shows the tie line power disturbance. By rejecting different disturbances and maintaining their frequency at the operating acceptable point while also effectively managing the tie line variation, the suggested SPSMCBSO was able to retain better resilience.

Remark 4.2. The response of the TAGHTPS has been subjected to simulations involving step load disturbances and random load variations, with the purpose of comparing it to the optimal controller presented in (G. Nidhi, K. Narendra, B. Chitti, 2019). The results of these simulations have demonstrated improvements. The results of these simulations affirm the robustness of the SPSMCBSO scheme as it effectively rejects these disturbances and maintains the stability of the TAGHTPS.

4.5.2 Simulation 2

Case 1: In this scenario, to assess the PS's behavior when subjected to the new algorithm, we introduce step load changes for both area 1 and area 2, in conjunction with wind speed variations as depicted in Figure 4.7. The proportion of wind energy in PS is on the rise that wind speed chart is displayed in Figures 4.8. However, the inherent fluctuations in renewable energy sources and variations in load can pose challenges for LFC. In this case, the wind power generation model is added to the PS. Both wind power generation model output power and load are uncertain.

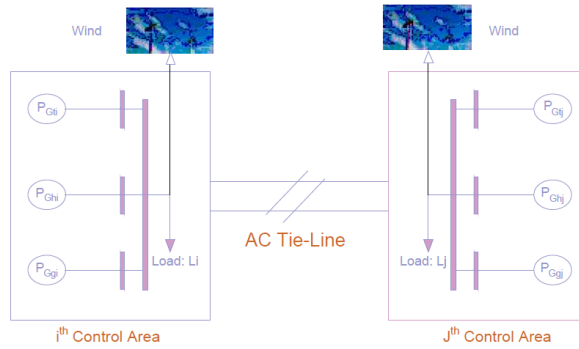


Figure 4.7. Two-area PS blocks schematic linked to a tie line

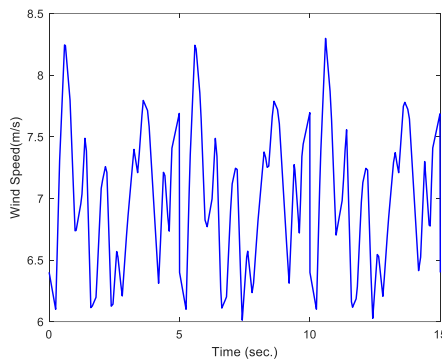


Figure 4.8. Wind speed chart (m/s).

Figures 4.9 and 4.10 show that the system frequency and tie line deviation of the SPSMCBSO can be reduced. So, it can be concluded that the fluctuation is caused by renewable energy and load disturbances. But by making use of the designed disturbance observer, the chattering of the SMLFC can be reduced.

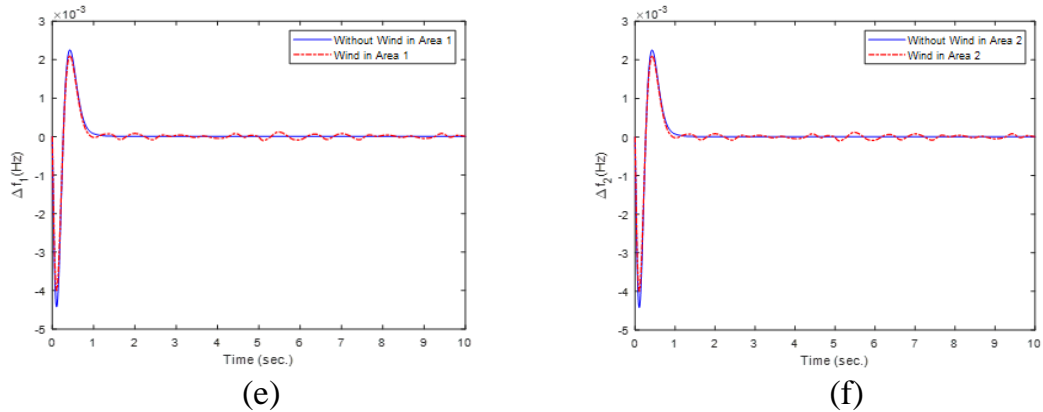


Figure 4.9. The frequency deviations [Hz] with 1.5% step load in area 1 (e) and area 2 (f) without and with wind speed variation.

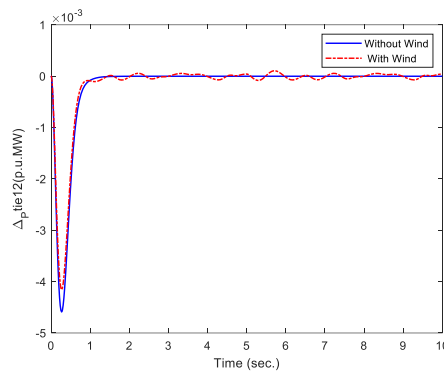


Figure 4.10. Tie line power deviation [p.u.MW].

So, it can be concluded that the fluctuation caused by renewable energy and load disturbances can be compensated effect through the designed SPSMCBSO.

4.6. Conclusion

This chapter introduces a novel approach called the SPSMCBSO for LFC in MAMSPS. The practicality and effectiveness of the SPSMCBSO technique are evaluated using the TAGHTPS model, which incorporates uncertainties in both state variables and interconnected parameters. The stability of the TAGHTPS system is rigorously established through a novel LMI approach based on Lyapunov theory. Comparative analysis of simulation results against recent methods demonstrates the superior performance of the SPSMCBSO approach. It is evident that the application of the suggested SPSMCBSO technique significantly enhances TAGHTPS's performance, surpassing the outcomes of previously utilized methods.

CHAPTER 5: SLIDING SURFACE DESIGN FOR SLIDING MODE LOAD FREQUENCY CONTROL OF MULTI AREA MULTI SOURCE POWER SYSTEM

In this chapter, a new second-order SMC via double integrated sliding surface (SOSDISS) is meant to improve MASHPS frequency regulation, tie-line power management, and dependability. Furthermore, the new LMI based on Lyapunov stability is used to analyze the entire MASHPS stabilization. Under parameter uncertainties and various assumed LDs from households, commercial buildings, and industries, the suggested SOSDISS proves to be highly robust and improves the MASHPS response in terms of frequency regulation, tie-line power management, and system reliability when compared to other existing proposed methods with less uncertainty consideration. The proposed control strategy's performance is effective and reliable, as evidenced by its fast frequency responses and insensitivity to parameter changes, load disturbance, load variation, delay time, and the GDB and GRC nonlinearity effects on PN, IEEE 39 bus.

5.1. Dynamic model of multi-area steam-hydropower system

To improve the stability and reliability of a multi-area steam-hydropower system (MASHPS), an LFC is needed.

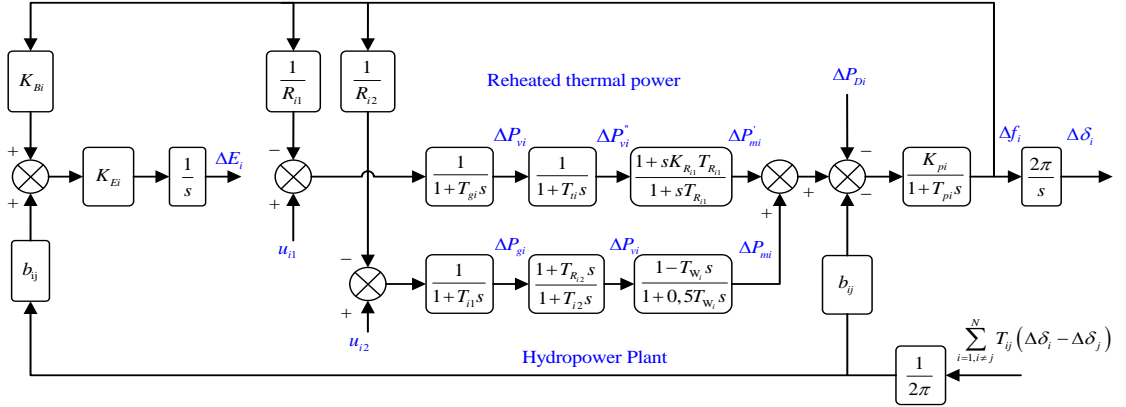


Figure 5.1. Schematic diagram of a 1-zone-2 sources included thermal power plants using heat recovery turbines & hydropower plant.

The LFC of the i^{th} area multi-source PS, which includes a reheated thermal power plant and a hydroelectric power plant and is presented in Figure 5.1. Therefore, we can represent the above dynamics in the state-space form below.

$$\dot{x}_i(t) = \bar{A}_{Ti}x_i(t) + \bar{B}_{Ti}u_i(t) + \sum_{\substack{j=1 \\ j \neq i}}^N \bar{H}_{Tij}x_j + \bar{F}_{Ti}\Delta\bar{P}_{TDi}(t) \quad (5.1)$$

Where $x_i(t) = [\Delta f_i(t) \ \Delta P_{mi}(t) \ \Delta P_{vi}(t) \ \Delta P_{gi}(t) \ \Delta E_i(t) \ \Delta \delta_i(t) \ \Delta P_{mi}'(t) \ \Delta P_{vi}''(t) \ \Delta P_{vi}'(t)]^T$

and $x_i(t) \in R^{n_i}$ is the vector of state, $u_i(t) \in R^{m_i}$ is the input control vector, $x_j(t) \in R^{n_j}$

is the neighboring state vector of $x_i(t)$, n_i is the area's total number of state variables. of i^{th} area, m_i is the area's total number of controls the input variables of the i^{th} area. $\bar{A}_{Ti} \in R^{n_i \times n_i}$, $\bar{B}_{Ti} \in R^{n_i \times m_i}$, $\bar{F}_{Ti} \in R^{n_i \times k_i}$ and \bar{H}_{Tij} are the nominal parameter system matrices. These are considered and represented in the system matrices and the control input, as shown bellowing as

$$\dot{x}_i(t) = [\bar{A}_{Ti} + \Theta_{Ti}(x_i, t)]x_i(t) + \bar{B}_{Ti}[u_i(t) + \xi_i(x_i, t)] + \sum_{\substack{j=1 \\ j \neq i}}^N [\bar{H}_{Tij} + \Xi_{ij}(x_j, t)]x_j(t) + \bar{F}_{Ti}\Delta\bar{P}_{TDi}(t) \quad (5.2)$$

where $\Theta_{Ti}(x_i, t)$ is the time varying parameter uncertainty in the state matrix, $\Xi_{ij}(x_j, t)$ is the interconnected matrix's time-varying parameter uncertainty and $\xi_i(x_i, t)$ is the disturbance input. If we simply uncertainties in equation (5.2), we can get that:

$$L_{Ti}(x_i, t) = \Theta_{Ti}(x_i, t)x_i(t) + \bar{B}_{Ti}\xi_i(x_i, t) + \sum_{\substack{j=1 \\ j \neq i}}^N \Xi_{ij}(x_j, t)x_j(t) + \bar{F}_{Ti}\Delta\bar{P}_{TDi}(t) \quad (5.3)$$

So, the state-space form of (5.3) can then be rewritten as

$$\dot{x}_i(t) = \bar{A}_{Ti}x_i(t) + \bar{B}_{Ti}u_i(t) + \sum_{\substack{j=1 \\ j \neq i}}^N \bar{H}_{Tij}x_j(t) + \bar{L}_{Ti}(x_i, t) \quad (5.4)$$

where $\bar{L}_{Ti}(x_i, t)$ represents the aggregate uncertainties which consists of the matched and mismatched parts. An assumption is made and formulated coupled with a given Lemma to handle the aggregate uncertainties for the LFC of MASHPS (5.4) as follows.

5.2. New double integral sliding surface design

A new double integral sliding surface has been designed as given.

$$\sigma_{Ti}[x_i(t)] = P_{Ti}x_i(t) - \int_0^t P_{Ti}(\bar{A}_{Ti} - \bar{B}_{Ti}\Lambda_{Ti})x_i(\tau)d\tau - \int_0^t \int_0^t P_{Ti}(\bar{A}_{Ti} - \bar{B}_{Ti}\Lambda_{Ti})x_i(\tau)d\tau d\tau \quad (5.5)$$

where P_{Ti} is the constant matrix and Λ_{Ti} is the design matrix, matrix P_{Ti} is chosen in order to ensure that matrix $P_{Ti}\bar{B}_{Ti}$ is nonsingular. The design matrix $\Lambda_{Ti} \in R^{m_i \times n_i}$ is chosen to satisfy the PS's inequality criterion (5.1).

$$\text{Re}[\lambda_{\max}(\bar{A}_{Ti} - \bar{B}_{Ti}\Lambda_{Ti})] < 0 \quad (5.6)$$

To determine the equivalent control, we differentiate $\sigma_{Ti}[x_i(t)]$ with respect to time as follows:

$$\begin{aligned} \dot{\sigma}_{T_i}[x_i(t)] &= P_{T_i}[\bar{A}_{T_i}x_i(t) + \bar{B}_{T_i}u_i(t) + \sum_{\substack{j=1 \\ j \neq i}}^N \bar{H}_{T_{ij}}x_j(t) + \bar{L}_{T_i}(x_i, t)] \\ &\quad - P_{T_i}(\bar{A}_{T_i} - \bar{B}_{T_i}\Lambda_{T_i})x_i(t) - \int_0^t P_{T_i}(\bar{A}_{T_i} - \bar{B}_{T_i}\Lambda_{T_i})x_i(\tau)d\tau \end{aligned} \quad (5.7)$$

So, by equating $\sigma_{T_i}[x_i(t)] = \dot{\sigma}_{T_i}[x_i(t)] = 0$. After that, the equivalent control is expressed by.

$$\begin{aligned} u_i^{eq}(t) &= -(P_{T_i}\bar{B}_{T_i})^{-1}[P_{T_i}\bar{A}_{T_i}x_i(t) + \sum_{\substack{j=1 \\ j \neq i}}^N P_{T_i}\bar{H}_{T_{ij}}x_j(t) + P_{T_i}\bar{L}_{T_i}(x_i, t) \\ &\quad - P_{T_i}(\bar{A}_{T_i} - \bar{B}_{T_i}\Lambda_{T_i})x_i(t) - \int_0^t P_{T_i}(\bar{A}_{T_i} - \bar{B}_{T_i}\Lambda_{T_i})x_i(\tau)d\tau] \end{aligned} \quad (5.8)$$

To close the loop system, we substitute $u_i^{eq}(t)$ into the equation (5.4) to yield the PS in the sliding motion with the following.

$$\begin{aligned} \dot{x}_i(t) &= (\bar{A}_{T_i} - \bar{B}_{T_i}\Lambda_{T_i})x_i(t) + [I_i - \bar{B}_{T_i}(P_{T_i}\bar{B}_{T_i})^{-1}P_{T_i}]\bar{L}_{T_i}(t) \\ &\quad + \sum_{\substack{j=1 \\ j \neq i}}^N [I_i - \bar{B}_{T_i}(P_{T_i}\bar{B}_{T_i})^{-1}P_{T_i}]\bar{H}_{T_{ij}}x_j(t) \\ &\quad + \int_0^t \bar{B}_{T_i}(P_{T_i}\bar{B}_{T_i})^{-1}P_{T_i}(\bar{A}_{T_i} - \bar{B}_{T_i}\Lambda_{T_i})x_i(\tau)d\tau \end{aligned} \quad (5.9)$$

Supporting that

$$\bar{z}_i(t) = \int_0^t x_i(\tau)d\tau; \quad \tilde{z}_i(t) = x_i(t) \quad (5.10)$$

We have

$$\dot{\tilde{z}}_i(t) = x_i(t) = \tilde{z}_i(t); \quad (5.11)$$

and

$$\begin{aligned} \dot{\bar{z}}_i(t) &= (\bar{A}_{T_i} - \bar{B}_{T_i}\Lambda_{T_i})\bar{z}_i(t) + [I_i - \bar{B}_{T_i}(P_{T_i}\bar{B}_{T_i})^{-1}P_{T_i}]\bar{L}_{T_i}(t) \\ &\quad + \sum_{\substack{j=1 \\ j \neq i}}^N [I_i - \bar{B}_{T_i}(P_{T_i}\bar{B}_{T_i})^{-1}P_{T_i}]\bar{H}_{T_{ij}}\tilde{z}_j(t) \\ &\quad + \bar{B}_{T_i}(P_{T_i}\bar{B}_{T_i})^{-1}P_{T_i}(\bar{A}_{T_i} - \bar{B}_{T_i}\Lambda_{T_i})\bar{z}_i(t) \end{aligned} \quad (5.12)$$

The preceding formula may be expressed as follows:

$$\begin{aligned}
\dot{\hat{z}}_i(t) = & \begin{bmatrix} 0 & I \\ \bar{B}_{T_i}(P_{T_i}\bar{B}_{T_i})^{-1}P_{T_i}(\bar{A}_{T_i}-\bar{B}_{T_i}\Lambda_{T_i}) & (\bar{A}_{T_i}-\bar{B}_{T_i}\Lambda_{T_i}) \end{bmatrix} \hat{z}_i(t) \\
& + \begin{bmatrix} 0 \\ [I_i - \bar{B}_{T_i}(P_{T_i}\bar{B}_{T_i})^{-1}P_{T_i}] \end{bmatrix} \bar{L}_{T_i}(t) \\
& + \sum_{\substack{j=1 \\ j \neq i}}^N \begin{bmatrix} 0 & 0 \\ 0 & [I_i - B_{T_i}(P_{T_i}\bar{B}_{T_i})^{-1}P_{T_i}]\bar{H}_{T_{ij}} \end{bmatrix} \begin{bmatrix} \bar{z}_j(t) \\ \tilde{z}_j(t) \end{bmatrix}
\end{aligned} \tag{5.13}$$

and

$$\dot{\hat{z}}_i(t) = \tilde{A}_{T_i}\hat{z}_i(t) + \tilde{F}_{T_i}\bar{L}_{T_i}(t) + \sum_{\substack{j=1 \\ j \neq i}}^N \tilde{H}_{T_{ij}}\hat{z}_j(t) \tag{5.14}$$

where $\hat{z}_i(t) = \begin{bmatrix} \bar{z}_i(t) \\ \tilde{z}_i(t) \end{bmatrix}$, $\tilde{F}_i = \begin{bmatrix} 0 \\ [I_i - B_i(P_i B_i)^{-1}P_i] \end{bmatrix}$,

$$\tilde{A}_i = \begin{bmatrix} 0 & I \\ \bar{B}_{T_i}(P_{T_i}\bar{B}_{T_i})^{-1}P_{T_i}(\bar{A}_{T_i}-\bar{B}_{T_i}\Lambda_{T_i}) & (\bar{A}_{T_i}-\bar{B}_{T_i}\Lambda_{T_i}) \end{bmatrix}, \text{ and } \tilde{H}_{ij} = \begin{bmatrix} 0 & 0 \\ 0 & [I_i - \bar{B}_{T_i}(P_{T_i}\bar{B}_{T_i})^{-1}P_{T_i}]\bar{H}_{T_{ij}} \end{bmatrix}$$

The above PS (5.14) is stable, which depends on the eigenvalue of the system matrices and the careful selection of the constant matrix gain P_{T_i} and design matrix gain Λ_{T_i} of the proposed equivalent control input. Furthermore, we analyze the stability of the PS using Lyapunov theory through LMI. To do this, we state the theorem as follows.

Theorem 5.1: The sliding motion (5.14) is asymptotically stable if and only if there are symmetric positive definite matrices M_i , $i=1, 2, \dots, N$, and positive scalars $\hat{\varepsilon}_i$, ε_i , δ_j and β_i and the following LMIs are obtained.

$$\begin{bmatrix} \tilde{A}_{T_i}^T M_i + M_i \tilde{A}_{T_i} + \sum_{\substack{j=1 \\ j \neq i}}^N \delta_j^{-1} \tilde{H}_{T_{ji}}^T \tilde{H}_{T_{ji}} & M_i & M_i \tilde{F}_{T_i} & M_i \bar{F}_{T_i} \\ M_i & -\hat{\varepsilon}_i^{-1} & 0 & 0 \\ \tilde{F}_{T_i}^T M_i & 0 & -\varepsilon_i & 0 \\ \bar{F}_{T_i}^T M_i & 0 & 0 & -\beta_i \end{bmatrix} < 0 \tag{5.15}$$

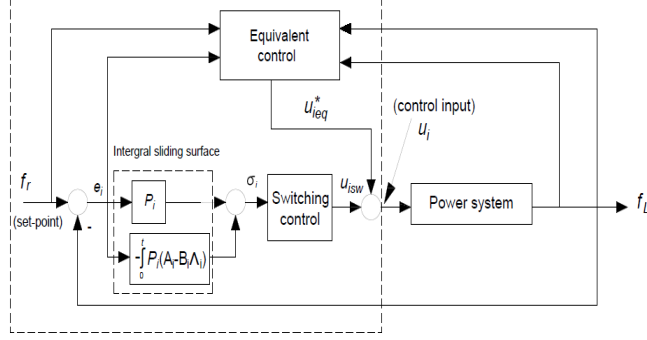


Figure 5.2. Simple diagram of traditional integral sliding surface.

Remark 5.1: The block diagrams of the aforesaid control techniques are shown in Figure 5.2 and Figure 5.3 to highlight the differences and improvements of the control methods, which include classic integral SMC. Under matched uncertainties, SMC based on first order double integral surfaces can be utilized to investigate the LFC of a PS in (R. Pradhan, B. Subudhi, 2015). However, in a real power network, parametric uncertainties do not always meet the matching condition. As a result, certain major limitations are required to build the first-order SMC to correct for uncertainties, which can guarantee nominal frequency convergence and system stability, but system trajectories cannot reach the origin point. As a result, the second-order double sliding surface approach is presented to push the system trajectory to an analogous point and improve transient performance.

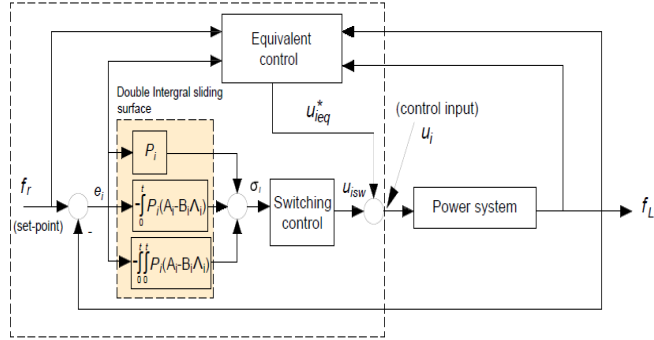


Figure 5.3. Simple diagram of the double integral sliding surface.

5.3. Decentralized continuous control law.

In this segment, the suggested decentralized second-order SMC law is suggested for LFC of the PS (5.9). The construction is done by simply making $\sigma_{Ti}[x_i(t)]$ and $\dot{\sigma}_{Ti}[x_i(t)]$ equal to zero (i.e., known as the sliding manifold) so that PS stability is improved.

In other words, the sliding manifold is defined and established $\Theta_{Ti}[\hat{z}_i(t)]$ as

$$\Theta_{Ti}(t) = \dot{\sigma}_{Ti}[x_i(t)] + \gamma_i \sigma_{Ti}[x_i(t)] \quad (5.16)$$

$$\text{and} \quad \dot{\Theta}_{Ti}(t) = \ddot{\sigma}_{Ti}[x_i(t)] + \gamma_i \dot{\sigma}_{Ti}[x_i(t)] \quad (5.17)$$

where $\gamma_i > 0$ is a positive constant. According to the formula (5.4), the equation (5.33) can be rewritten as

$$\begin{aligned} \dot{\Theta}_{T_i}(t) = & P_{T_i}[\bar{A}_{T_i}\dot{x}_i(t) + \bar{B}_{T_i}\dot{u}_i(t) + \sum_{\substack{j=1 \\ j \neq i}}^N \bar{H}_{T_{ij}}\dot{x}_j(t) + \dot{\bar{L}}_{T_i}(x_i, t)] - P_{T_i}(\bar{A}_{T_i} - \bar{B}_{T_i}\Lambda_{T_i})\dot{x}_i(t) \\ & - P_{T_i}(\bar{A}_i - \bar{B}_{T_i}\Lambda_{T_i})x_i(t) + \gamma_i\dot{\sigma}_{T_i}[x_i(t)] \end{aligned} \quad (5.18)$$

If the sliding manifold is made equal to zero, then the proposed decentralized SMC is given as

$$\begin{aligned} \dot{u}_i(t) = & -(P_{T_i}\bar{B}_{T_i})^{-1}\{\|P_{T_i}\|\|\bar{A}_{T_i}\|\|\dot{x}_i(t)\| + \sum_{\substack{j=1 \\ j \neq i}}^N \|P_{T_j}\|\|\bar{H}_{T_{ji}}\|\|\dot{x}_i(t)\| \\ & + \|P_{T_i}\|\|(\bar{B}_{T_i}\Lambda_{T_i} - \bar{A}_{T_i})\|\|\dot{x}_i(t)\| + \|P_{T_i}\|\|(\bar{B}_{T_i}\Lambda_{T_i} - \bar{A}_{T_i})\|\|x_i(t)\| \\ & + \gamma_i\|\dot{\sigma}_{T_i}[x_i(t)]\| + \|P_{T_i}\|\bar{\gamma}_i + v_i\} \frac{\Theta_{T_i}^T(t)}{\|\Theta_{T_i}(t)\|} \end{aligned} \quad (5.19)$$

To satisfy the above proposed control input (5.19), the system variables trajectories must be forcefully driven to the sliding manifold (SM) and remain therein at finite reaching time to ensure the PS's asymptotic stability (5.9) asymptotic stability. Therefore, we again analyze the stability of the system by the given theorem.

5.4. Case studies and simulation results.

In this part, the suggested second-order SMC via double integral sliding surface is put into practice for the LFC of a TASHPS respectively. The proposed controller performance is validated when the various simulation results are compared with recent methods, which are briefly discussed in different simulations under various conditions as follows.

5.4.1. Simulation 1

Case 1: The proposed SMC is tested in a TASHPS with choosing the same step load disturbance and system parameters as in (J. Srilekha, C.N. Kalyan, G. Stanley, K. Suneetha, M.M. Thakreem, 2020). Figures 5.4 (a) and 5.4 (b) give the control area 1 and 2 frequency variations. The TASHPS tie-line power is shown in Figure 5.5. From the analysis of both results, both frequencies undershoot did not exceed the tolerable point of -0.5Hz. Therefore, implies the proposed SMC is superior to the GWO based fuzzy PID method regarding control performance.

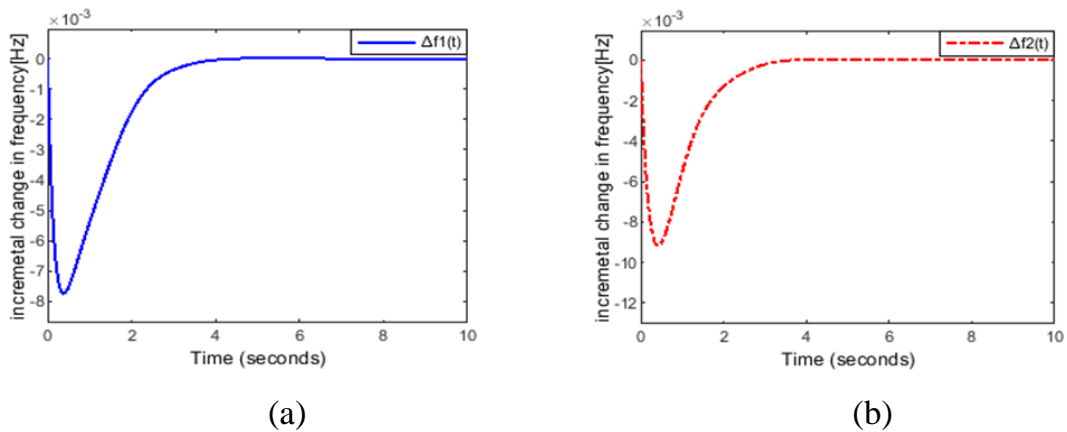


Figure 5.4. Frequency [Hz] (a) and (b) of control area 1 and 2 under matched disturbances.

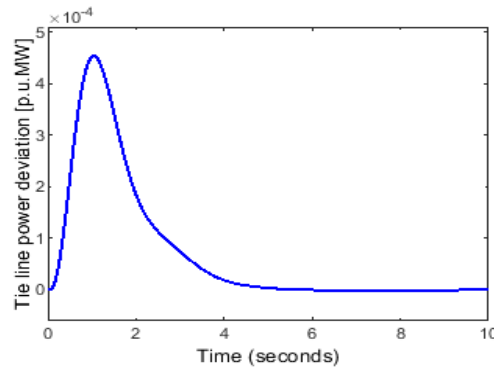


Figure 5.5. Tie line power deviation [p.u.MW] with matched disturbances.

Remark 5.2: Notably, as can be seen in (J. Srilekha, C.N. Kalyan, G. Stanley, K. Suneetha, M.M. Thakreem, 2020), the new controller is more resilient to load disturbances and responds more quickly.

Case 2: Given this, we consider a change in the load demand from commercial business buildings in a metropolitan city. The commercial buildings load demand from CA 1 and 2 of the TASHPS is given in (J. Srilekha, C.N. Kalyan, G. Stanley, K. Suneetha, M.M. Thakreem, 2020). The demand curve is plotted and shown in Figure 5.6. As the demands change, as seen from the load curve, the dynamics responses of the TASHPS change. Figure 5.7 (c) shows the frequency variation of both control area 1 and area 2 whereas Figure 5.7 (d) illustrates the TASHPS tie-line power deviation.

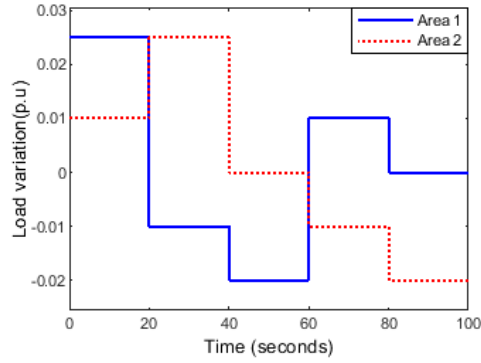


Figure 5.6. Daily load curve of commercial business buildings

From the Figs, the TASHPS dynamics is improved regarding far little under/overshoot and settling time, which did not exceed the tolerable point given in (J. Srilekha, C.N. Kalyan, G. Stanley, K. Suneetha, M.M. Thakreem, 2020). This further makes the proposed method capable of handling LFC of large PS to keep the PS stable and reliable.

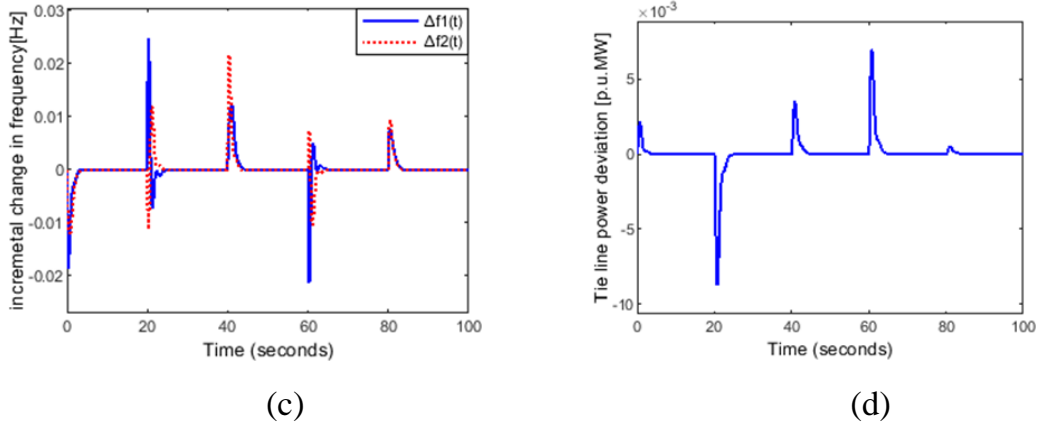


Figure 5.7. Control area 1 and control area 2 frequency deviation (c) and TASHPS tie line power deviation (d).

Remark 5.3: The SMC chattering issue is particularly harmful to the PS actuators. The suggested controller generates the correct signal and employs energy to make up for frequency damping in the primary control, which consists of a governor. Consequently, the governor's droop control of speed will accurately activate the valve, supplying needed steam to the turbine to increase mechanical inertia power to match the load change or requirement. As a result, the setup time is short, and the overshoot is negligible.

5.4.2. Simulation 2:

Case 1: In this scenario, a bigger and more realistic PS, the New England 10-generator 39-bus PS, is used to further evaluate the performance of the suggested LFC scheme. The New England test system consists of ten generators, 39 buses, nineteen loads, 34 lines for transmission, and twelve transformers. Figure 5.8 depicts a single-line schematic of the test system taken from (K. Liao, Y.A. Xu, 2017).

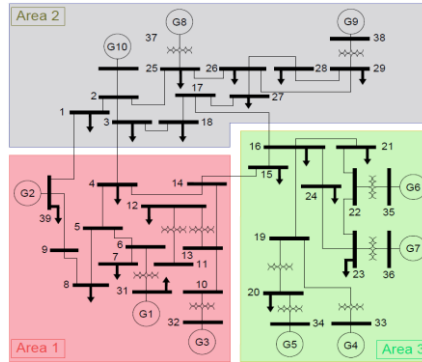


Figure 5.8. The block diagram of the New England 39 bus system

As the load demands in a real PS fluctuate, we used a random load fluctuation at each location, as seen in Figure 5.9. Figure 5.10 (e) depicts the frequency fluctuation of areas 1, 2, and 3, respectively, while Figure 5.10 (f) depicts the power deviation.

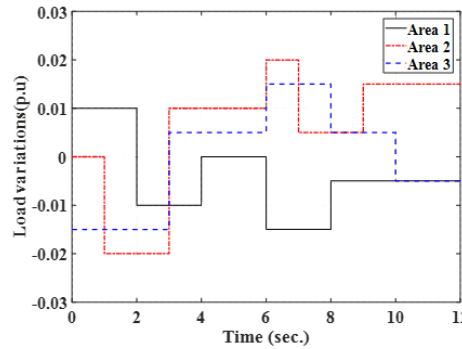


Figure 5.9. Random load variation

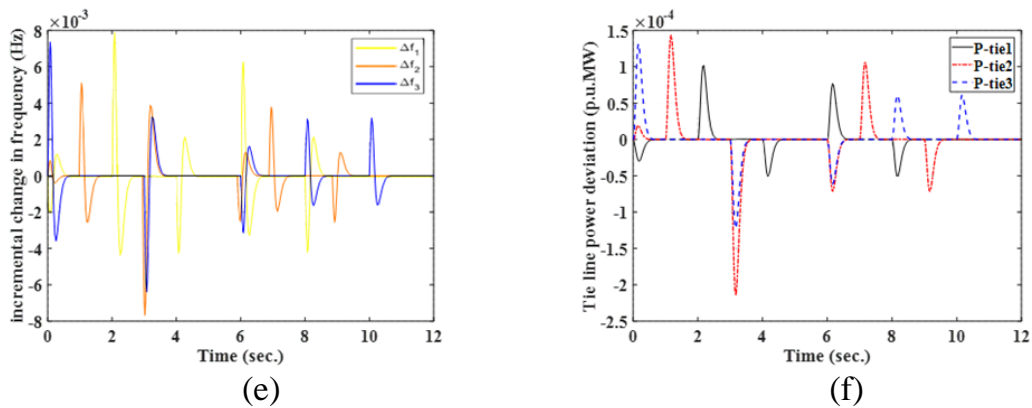


Figure 5.10. The dynamic responses of the frequency deviation and the tie-line power

Remark 5.4. In summary, the suggested novel technique provided higher control performance in terms of maintaining tie-line power and frequency at the approved point for the PS where system state variables are hard to quantify. The suggested approach is incredibly powerful, not only reducing chattering but also ensuring the MAPS's resilience.

Case 2: In particular, due to its non-linearity, the GRC has a detrimental impact on PN performance with the same step load disturbance and system parameters as in (J. Srilekha, C.N. Kalyan, G. Stanley, K. Suneetha, M.M. Thakreem, 2020). Figure 5.11 (K. Liao and Y. Xu, 2018) depicts a nonlinear governor model with GDB and a nonlinear turbine model with GRC applied in the TASHSP.

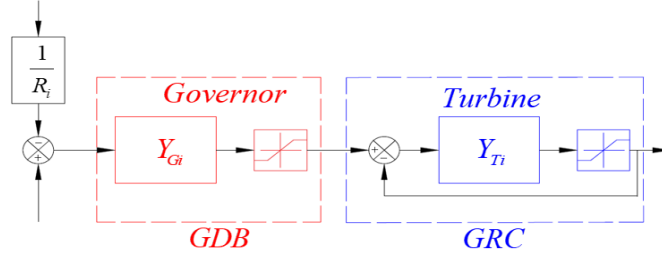
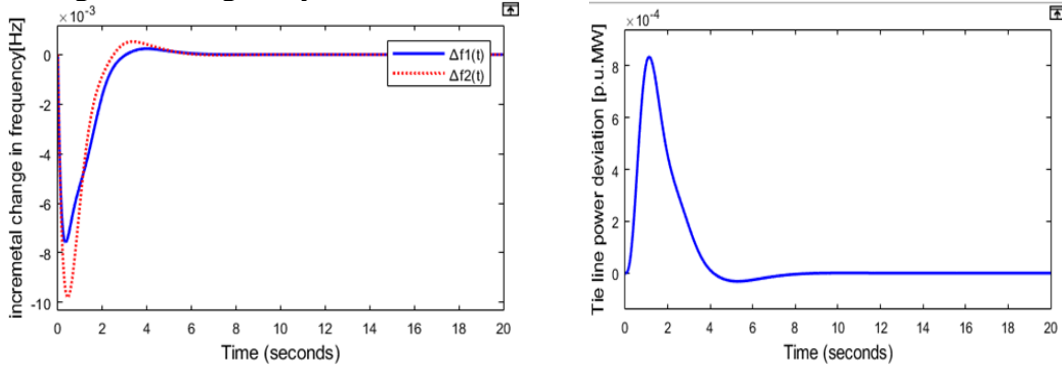


Figure 5.11. Nonlinear governor model with dead band and Nonlinear turbine model with the GRC in paper

Figures 5.12 (g) and 5.12 (h) show the frequency and tie-line power variations. As can be seen, with the suggested SOSDISS controllers, transient oscillations are determined for a longer time and with a bigger amplitude than in Case 1 in Simulation 1. In contrast to (J. Srilekha, C.N. Kalyan, G. Stanley, K. Suneetha, M.M. Thakreem, 2020) and Simulation 1 with Case 1, the suggested control approach was found to be adequate even in the presence of GRC, GDB, and step load disturbances. In the transient performance of the proposed SOSDISS controller, the % overshoot and the settling time are greatly reduced under the GDB and GRC effects.



(g)

(h)

Figure 5.12. The frequency responses and dynamic responses of the tie-line power of two areas with GRC and GRB.

Remark 5.5: The simulation results are used to compare Simulation 1 with Case 1 of considering or without considering the nonlinearity effects of GDB and GRC in to (J. Srilekha, C.N. Kalyan, G. Stanley, K. Suneetha, M.M. Thakreem, 2020) to demonstrate the robustness of the proposed SOSDISS. In contrast to previous studies, the suggested SOSDISS controller, as a result, the planned SOSDISS's tiny frequency fluctuations have less impact on plant reserve capacity and the electricity market.

Case 3: Because the same parameter uncertainty of the three regions MAPS

is employed in Case 1 of Simulation 1, the nominal operating point is used to test the usefulness and resilience of the proposed controller to load disturbance. Figures 5.13 (a) and 5.13 (b) show the fast decrease of the tie-line power and frequency disturbance.

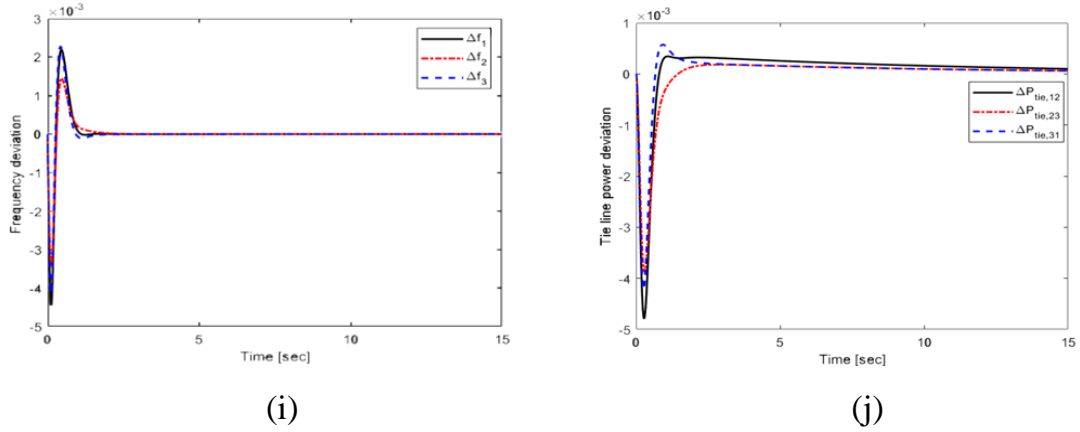


Figure 5.13. The dynamic responses of frequency change and tie line power in three areas.

Figure 5.21. As a result, the suggested SOSDISS controller is applied for three-area multisource multi-area PS. It also shows that the SOSDISS can stabilize the system in conjunction with the large system. When the simulation results are compared, the suggested double sliding switching surface and the planned SOSDISS can eliminate overshoot, improve reaction speed, and restrict frequency variation to zero.

5.4.3. Simulation 3:

The proposed LFC based on SOSDISS has been examined with different effects of step load disturbance on the MAPS with nominal parameter conditions in to (J. Srilekha, C.N. Kalyan, G. Stanley, K. Suneetha, M.M. Thakreem, 2020) and time delay in (Y. Mi, X. Hao, Y. Liu, Y. Fu, C. Wang, P. Wang and P.C. Loh, 2017). The three-area restructured PS in Figure 5.14 has a transmission time delay.

Remark 5.6. The findings of the testing simulation are assigned in this section on Figures 5.15 (k) to 5.15 (l). Particularly when time-delay communication is considered for the large-scale PN, the report of findings can demonstrate in an effective comparison. As a result, the recommended SOSDISS's system performance is well balanced, and frequency variation is 0 after 1s.

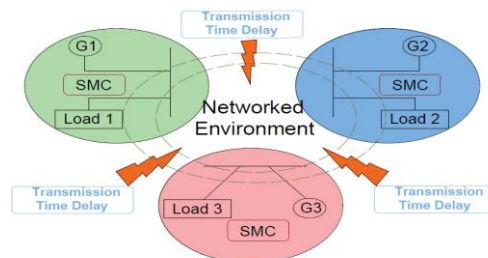


Figure 5.14. A three-area restructured PS with transmission time delay.

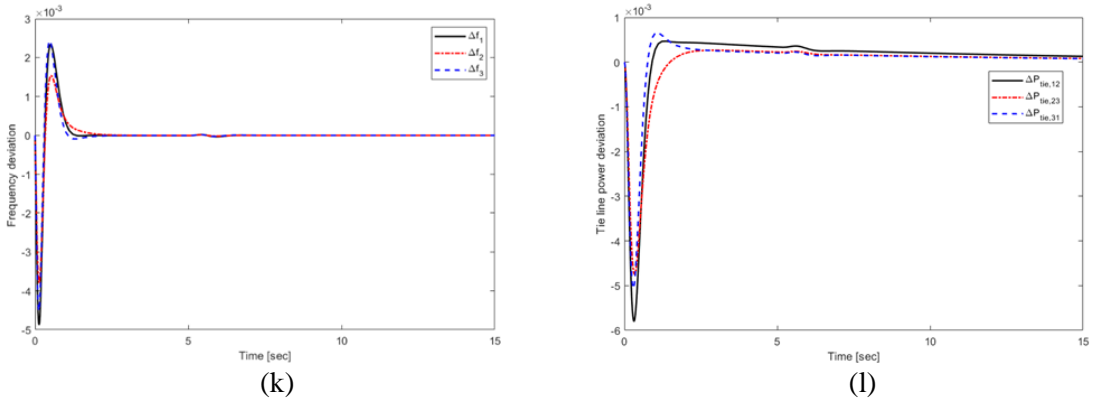


Figure 5.15. Frequency deviation and Tie-line deviation with time delay at $\tau = 5s$

5.5. Conclusion.

In conclusion, an LFC study based on the proposed LFC method is developed with a SOSDISS. On the other hand, a decentralized SOSDISS is given with carefully selected matrices gains to improve the PS asymptotic stability and reduces chattering inherent in first-order SMC. The novel LMI based on Lyapunov theory, in which the derivative of the Lyapunov function is smaller than zero, is used to examine the asymptotic stability of the PS. To test large scale PS, the proposed second-order SMC appears to be capable of handling the PS's LFC, making it suitable for MASHPS frequency regulation and PS reliability. There are no assumptions about the distributions of the dynamics/bandwidth of the communication network with packet loss or the constraints of the controlled plants to evaluate the performance of SMC for disturbances with frequency domain specifications of networked control systems. In the future, we will focus on new SMCs for various disturbances with frequency domain requirements to evaluate the performance of the networked PS or will consider dynamics of the communication network considering the impact of packet loss.

CHAPTER 6: CONCLUSION AND RECOMMENDATIONS FOR FUTURE WORK

6.1. Conclusion

Multiple secondary frequency control strategies were developed based on different theories to ensure the maintenance of frequency within acceptable limits in two distinct testbed systems. In pursuit of the highest dynamic performance, various innovative SMC schemes were employed for optimization. These includes second-order integral sliding mode control (SOISMC), single-phase sliding mode control-based state observer (SPSMCBSO), and a second-order SMC approach using double integral sliding surfaces (SOSDISS).

6.2. Recommendations for future work

This study might be expanded in the following areas in future work:

1. In our current research, we operate under the assumption that PS control areas comprise a diverse mix of power generation sources, including thermal, hydro, and gas resources within each area. In the future studies, this expanded perspective might encompass the integration of diverse sources such as gas, wind, diesel, nuclear, energy storage systems, and other components within each control area of a multi-area multisource PS, restructured PS environment.

2. Given the rapid response provided by the suggested SMC, it would be prudent to conduct further investigations to assess the system's stability under varying operating conditions. It is well-established that an exceedingly fast response carries the risk of inducing system oscillations, making this an important aspect to examine.

3. Examining alternative AI algorithms such as Differential Evolution, Bees Algorithm, and Cuckoo Search to fine-tune the suggested SMC controllers and evaluating their potential to enhance the dynamic performance of these controllers is a valuable direction for further research. .

4. Continuing research into the development of combined fuzzy and SMC controllers, with the optimization of membership functions through advanced techniques, has the potential to greatly improve the overall performance of novel fuzzy logic controllers.

5. Demand-side frequency response represents another effective approach that warrants further investigation into controlling frequency within the PS. Therefore, delving deeper into this topic and offering novel solutions presents a promising avenue for frequency control research. These methods can potentially be extended to LFC studies of micro-grids, with the inclusion of various energy storage devices for enhanced control and stability.

REFERENCES

- Momoh, J. A. (2017). *Electric power system applications of optimization*. CRC press.
- A. J. Wood and Bruce F. Wollenberg Gerald B. Sheblé. (2014). *Power Generation, Operation, and Control*. New Jersey: Wiley.
- A.T. Tran, B.L.N Minh, V.V. Huynh, P.T. Tran, E.N. Amaefule, V.D. Phan, T.M Nguyen, (2021). Load frequency regulator in interconnected power system using second order sliding mode control combined with state estimator. *Energies*, 863.
- Asghar, R., Riganti Fulginei, F., Wadood, H., & Saeed, S. (2023). A review of load frequency control schemes deployed for wind-integrated power systems. *Sustainability*, 8380.
- B. Le Ngoc Minh, V. V. Huynh, T. M. Nguyen, and Y. W. Tsai, (2018). Decentralized adaptive double integral sliding mode controller for multi-area power systems. *Mathematical Problems in Engineering*, 11.
- B. M. Weedy, B. J. Cory, N. Jenkins, J. B. Ekanayake, and G. Strbac, (2015). *Electric Power Systems*, Fifth Edition. West Sussex: John Wiley & Sons Ltd.
- Bevrani, H. (2014). *Robust Power System Frequency Control*. Cham: Springer International Publishing.
- Boyd, S.; Ghaoui, E.L.; Feron, E.; Balakrishna, V. (1994). *Linear Matrix Inequalities in System and Control Theory*. Philadelphia, Pennsylvania, USA: SIAM.
- Casavola, A., Franzè, G., & Tedesco, F. (2023). Centralized supervision and coordination of load/frequency control problems in networked multi-area power systems. *In Electric Transportation Systems in Smart Power Grids*, 375-423.
- D. Guha, P.K. Roy, S. Banerjee, (2020). Quasi-oppositional JAYA optimized 2-degree-of-freedom PID controller for load-frequency control of interconnected power systems. *International Journal of Modelling and Simulation*, 1–23.
- Devendra, K. (2008). *Techniques and Its Applications in Electrical Engineering*. Berlin/Heidelberg, Germany: Springer.
- Edris, A. A., & D'Andrade, B. W. (2017). *Transmission grid smart technologies*. In *The power grid*. Academic Press.
- F.Guo, (2020). Application of a novel adaptive sliding mode control method to load frequency control". *European Journal of Control*, 172-178.
- Guo, J. (2019). Application of full order sliding mode control based on different areas power system with load frequency control. *ISA transactions*, 23-34.
- Gupta, D. K., Jha, A. V., Appasani, B., Srinivasulu, A., Bizon, N., & Thounthong, P. (2021). Load frequency control using hybrid intelligent optimization technique for multi-source power systems. *Energies*, 1581.
- H. Bevrani, (2014). *Robust power system frequency control*. Springer.
- H. Bevrani, H. Golpîra, A. R. Messina, N. Hatziargyriou, F. Milano. (2021). Power system frequency control: An updated review of current solutions and new challenges. *Electric Power Systems Research*, 194.
- H. Yousef. (2015). Adaptive fuzzy logic load frequency control of multiarea power system. *International Journal of Electrical Power & Energy Systems*, 384–

395.

Huynh, V. V., Minh, B. L. N., Amaefule, E. N., Tran, A. T., Tran, P. T., Phan, V. D., & Nguyen, T. M. (2021). Load Frequency Control for Multi-Area Power Plants with Integrated Wind Resources. *Applied Sciences*, 3051.

Ismayil, C., Sreerama, K. R., & Sindhu, T. K. (2014). Automatic generation control of single area thermal power system with fractional order PID ($PI\lambda D\mu$) controllers. *IFAC proceedings volumes*, 552-557.

J. Guo. (2021). Application of a novel adaptive sliding mode control method to the load frequency control. *European Journal of Control*, 172-178.

Le, N. M. B.; Van, V. H.; Nguyen, T. M.; Tsai, Y. W. (2018). Decentralized adaptive double integral sliding mode controller for multi-area power systems. *Mathematical Problems in Engineering*, 1–11.

M. Vijay, C. James, A. Paul, A. Fouad, (2019). *Power system control and stability*. Hoboken, New Jersey, USA: Wiley-IEEE Press.

Mi, Y.; Fu, Y.; Li, D.; Wang, C.; Loh, P.C.; Wang, P. (2016). The sliding mode load frequency control for hybrid power system based on disturbance observer. *Int. J. Electr. Power Energy Syst.*, 446–452.

Prabha S. Kundur, O. M. (2022). *Power System Stability and Control, Second Edition*. McGraw Hill; 2nd edition.

S. Prasad, S. Purwar, and N. Kishor, (2019). Load frequency regulation using observer-based nonlinear sliding mode control. *International Journal of Electrical Power & Energy Systems*, 178-193.

Sahu, R. Kumar, P. Sidhartha, Rout, U. Kumar, Sahoo, D. Kumar. (2016). Teaching learning-based optimization algorithm for automatic generation control of power system using 2-DOF PID controller. *International Journal of Electrical Power & Energy Systems*, 287-301.

V.V. Huynh, B.L.N Minh, B.L.N, E.N. Amaefule, A.T. Tran, P.T. Tran, V.D. Phan, V.T. Pham, T.M. Nguyen. (2021). Load frequency control for multi-area power plants with integrated wind resources. *Applied Sciences*, 7.

V.V. Huynh, P.T. Tran, B.L.N. Minh, Tran, A.T. Tran, T.M. Nguyen, P.T. Vu, (2020). New second-order sliding mode control design for load frequency control of a power system. *Energies*, 24.

Vijay, V.; James, C; Paul, A; Fouad, A. (2019). *Power system control and stability*. Hoboken, New Jersey, USA: Wiley-IEEE Press.

VV, Huynh, BNL Minh, EN Amaefule, A.T. Tran, T.P. Tran, (2021). Highly robust observer sliding mode-based frequency control for multi-area power systems with renewable power plants. *Electronics*, 274.

Y. Mi, F. Yang, D. Li, C. Wang, L.P. Chiang, W. Peng. (2016). The sliding mode load frequency control for hybrid power system based on disturbance observer. *Electrical Power and Energy Systems*, 446-452.

Y. Mi, X. Hao, Y. Liu, Y. Fu, C. Wang, P. Wang and P.C. Loh, (2017). Sliding mode load frequency control for multi-area time-delay power system with wind power integration. *IET Generation, Transmission & Distribution*, 4644–4653.